HAVSTOVAN
FAROE MARINE RESEARCH INSTITUTE

Monitoring the velocity structure of the Faroe Current

Tórshavn · May 2019
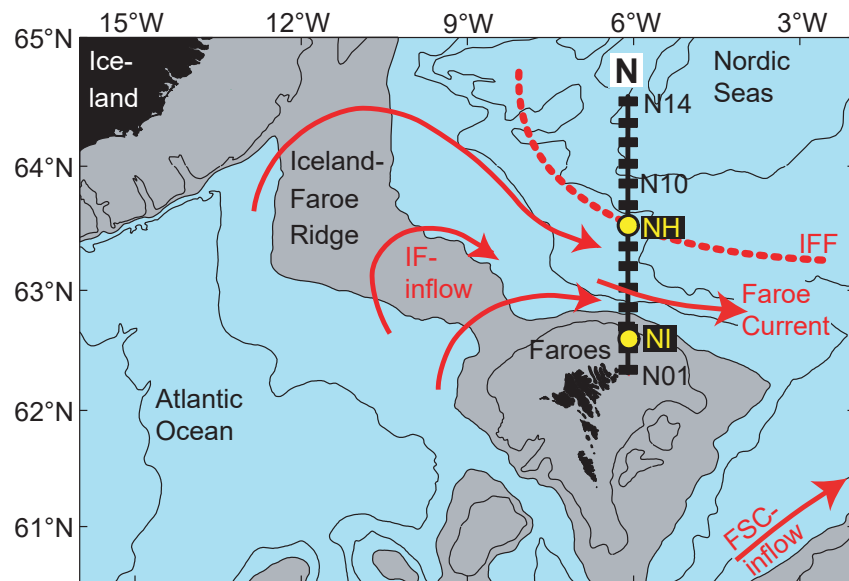
Bogi Hansen

Karin Margretha Húsgarð Larsen

Hjálmar Hátún

Monitoring the velocity structure of the Faroe Current

Bogi Hansen, Karin Margretha Húsgarð Larsen, and Hjálmar Hátún

Abstract

This report is intended to document continuing efforts to optimize the monitoring of volume, heat, and salt transport in the Faroe Current. The present monitoring system is based on a combination of in situ observations and data from satellite altimetry as documented by Hansen et al. (2015). The altimetry data are freely available, whereas in situ observations are costly in equipment, ship-time, and manpower. Efforts have therefore continuously been made to reduce the reliance on in situ observations.

Although the altimetry data have become a very useful tool for analyzing variations in surface velocity, they do have three major problems: (1) Due to uncertainties in the geoid, absolute surface velocities based solely on altimetry are not reliable. (2) A priori, the altimetry data only apply to surface, not subsurface, velocities. (3) Altimetry data have no direct information on the temperature and salinity distributions.

In this report, we address the first two of these problems. By using the complete data set of in situ observations, especially current measurements from moored ADCPs, we are able to calibrate the altimetry data so that they give reliable surface velocities, solving problem (1). These observations furthermore show that the vertical variations in velocity are sufficiently consistent that subsurface velocities and transport values can be derived from surface velocity, and hence altimetry, throughout the layer of Atlantic water on the section on monthly time scales or longer, solving problem (2).

Based on the analysis presented, we therefore conclude that in situ current measurements are no longer necessary to monitor the velocity structure of the Faroe Current, although we recommend that one of the long-term ADCP mooring sites is maintained to guard against potential drastic changes in the system. The new information has been incorporated into the algorithms for deriving transport time series, but the differences between the new time series and previously published time series are minimal.

This leaves the third problem: monitoring the temperature and salinity fields. We have a large historical data set from ship-borne observations and moored temperature sensors, but a central component is missing. This is the data from two moored PIES (Pressure Inverted Echo Sounders), borrowed from the University of Hamburg, which due to German cruise cancelations, bad weather conditions, and instrument malfunction have not yet been recovered. The decision on how to monitor the temperature and density structure, and how to use this information to determine Atlantic water transport, is therefore delayed and will be treated in a second report, planned to be finalized later in 2019.

1 Introduction

The inflow of Atlantic water to the Nordic Seas between Iceland and the Faroes becomes focused into a relatively narrow boundary current north of the Faroes, termed the Faroe Current (Figure 1). Since the late 1980s, hydrographic properties of this current have been monitored by regular CTD observations at a fixed set of standard stations N01 to N14 along a section, the N-section, that follows the 6.083°W meridian.
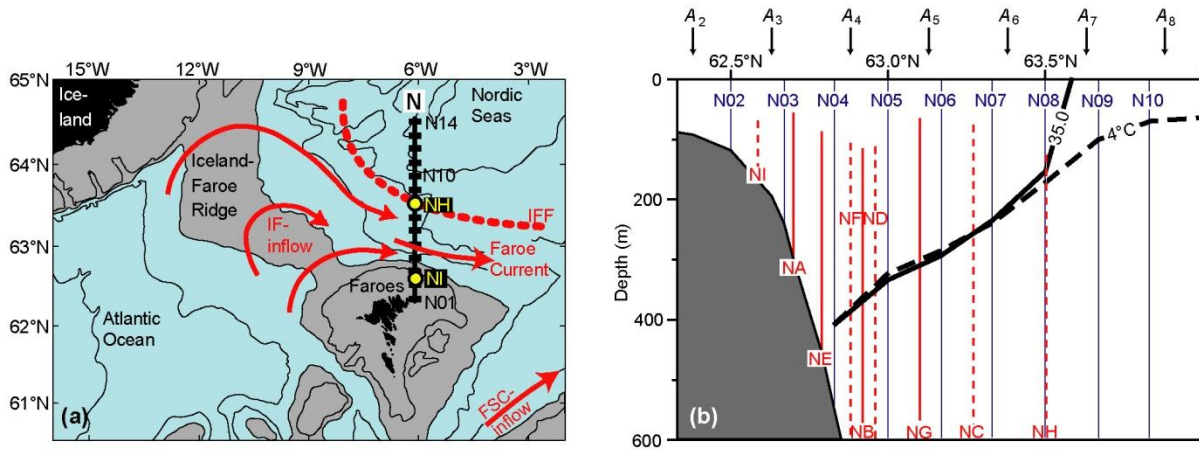
Figure 1. (a) The region between Iceland and the Scottish shelf with grey areas shallower than 500m. The two main Atlantic inflow branches are indicated by red arrows. The Iceland-Faroe inflow (IF-inflow) crosses the IFR, meets colder waters, termed Arctic water, in the Iceland-Faroe Front (IFF), and flows north of Faroes in the Faroe Current. The other main inflow branch (the FSC-inflow) is also shown. The black line extending northwards from the Faroe shelf is the N-section with CTD standard stations N01 to N14 indicated by black rectangles. Yellow circles indicate the innermost (NI) and the outermost (NH) ADCP mooring sites on the section. **(b)** The southernmost part of the N-section with bottom topography (grey). CTD standard stations are indicated by blue lines labelled N02 to N10. ADCP profiles are marked by red lines that indicate the typical range with continuous lines indicating the long-term sites. Altimetry grid points A_2 to A_8 are marked by black arrows and the thick black lines indicate the average depth of the 4 °C isotherm (dashed) and the 35.0 isohaline (continuous) on the section (from Hansen et al., 2015).

In the mid-1990s, the hydrographic observations were complemented by regular deployments of upward looking ADCPs (Acoustic Doppler Current Profilers) along the section (Figure 1). These deployments have mainly been repeated at some fixed sites, but in addition, single deployments have been located at other sites.

The main aim of these observations has been to monitor transports of volume (water, mass), heat, and salt in the Faroe Current and, originally, the estimated transport values were based purely on the in situ measurements (ADCP and CTD observations), but these estimates were found to correlate remarkably well with sea-level data from satellite altimetry (Hansen et al., 2010). Altimetry data and ADCP data also complement one another well and a new strategy was adopted, which is based on combining altimetry data and in situ data. The original implementation of this strategy is documented in Hansen et al. (2015), but it was clear from the outset that the algorithms for deriving transport values from the observations could be refined.

To realize this, additional dedicated in situ observations have been carried out as well as more extensive analysis of existing observational data. These activities have been made possible within the FARMON project, funded by the Danish Energy Agency as part of the Arctic Climate Support Programme. A complete revision of the present set of algorithms may be split into three separate tasks:

1. **Calibration of altimetry data to give accurate surface velocities.** This mainly involves comparing altimetry data with simultaneous data from ADCP measurements that are extrapolated to the surface. For most of the monitoring section, this was done from existing ADCP data by Hansen et al. (2015), but parts of the section were not well covered by ADCP deployments. Since then, additional ADCP data have been acquired at two new deployment sites, which allows refinement of the altimetry calibration.

2. **Determining the vertical velocity variation from surface velocity and altimetry.** Calculating transport involves integration of the velocity field both horizontally and vertically and this requires knowledge of the vertical variation of the velocity. Since the development of the existing algorithms for that purpose, additional ADCP data have been acquired both at the two new ADCP sites and at three long-term ADCP deployment sites, which should allow refinement of the algorithms for calculating the velocity field.

3. **Determining the hydrographic structure and the depth of the Atlantic layer along the monitoring section**. In order to distinguish the volume transport of Atlantic water from the other water masses flowing through the monitoring section, the temporal variation of the depth of the Atlantic water layer along the section has to be derived from the available observational data. Calculating transport of heat and salt furthermore requires knowledge of the temporal variations of the temperature and salinity fields on the section.

These three tasks have been planned to be carried out within the FARMON project. For tasks 1 and 2, all the planned observations have been completed and their development into updated algorithms will be documented in this report. As part of task 3, two PIES (Pressure Inverted Echo Sounder) were kindly supplied by the University of Hamburg (UHAM) and deployed in 2017. Originally, they were planned to be recovered by UHAM in 2018, but the planned recovery cruise by UHAM was cancelled. A planned recovery by R/V Magnus Heinason in February 2019 also had to be cancelled due to bad weather conditions and an attempt in early May 2019 failed due to malfunction of the acoustic release deck unit.

This has made it necessary to delay the analysis of the hydrographic fields on the monitoring section and this report will therefore focus purely on the velocity field and how to combine altimetry and ADCP data into algorithms that allow its determination. As outlined in the abstract, this can be split into two tasks (Task 1 and Task 2), which will be treated separately in the following. In the text, we will refer repeatedly to Hansen et al (2015) and this reference is therefore abbreviated to "H2015".

2 Data

Most of the data analyzed in this report are from ADCP deployments and from satellite altimetry. The ADCP data have been acquired at nine separate sites along the monitoring section. The deployment sites are labelled with two-letter codes where the first letter (N) refers to the section (Table 1). More detailed information on individual deployments is found in Table A1 in the appendix. ADCP data from seven of these sites were reported in H2015, but only up to May 2014. At sites NA, NB, and NG, additional data have been acquired and two new sites (NI and NH) have been occupied by one deployment at each of the sites. The four sites that have been most frequently occupied (NA, NE, NB, and NG) will be referred to as the "long-term" ADCP sites.

The velocity data from the ADCPs are structured in "bins" (i.e. depth intervals), which in our case have been either 10 m or 25 m (column labelled "Lgt" in Table A1). Usually, the ADCPs have been programmed to ping every 20 minutes. The raw data have been processed, edited, de-tided, and averaged to daily values. The highest level with 100% "good" daily averaged data (i.e. not error flagged) throughout the deployment period is listed for each deployment in the columns labelled "Top" in Table A1, but individual days may reach higher and the columns labelled "Last" in Table A1 list the very highest level reached for each deployment. For days with error flagged bins below the highest good bin, these were interpolated vertically. Finally, velocities were interpolated vertically to meter intervals.

Table 1. Main characteristics of the measurements at the nine ADCP sites and their locations in altimetry intervals.

Site	Latitude	Bottom depth (m)	Period	Number of depl.	Number of days	Distance from N02	Altimetry interval
NI	62.58°N	156	Jun 2017 - May 2018	1	342	9 km	A_2-A_3
NA	62.70°N	300	Jun 1996 - May 2015	20	6663	22 km	A_3-A_4
NE	62.79°N	455	Jul 2000 - May 2011	8	2729	32 km	A_3-A_4
NF	62.88°N	700	Jul 2000 - Jun 2001	1	343	42 km	A_4
NB	62.92°N	925	Oct 1994 - May 2018	24	7272	47 km	A_4-A_5
ND	62.96°N	1280	Nov 1997 - Jun 1998	1	213	51 km	A_4-A_5
NG	63.10°N	1815	Jul 2000 - May 2015	14	4788	67 km	A_4-A_5
NC	63.27°N	1730	Oct 1994 - Jun 2000	5	1517	85 km	A_5-A_6
NH	63.50°N	1802	Jun 2015 - May 2016	1	339	111 km	A_6-A_7

Daily averaged altimetry was selected from the global gridded (0.25°x0.25°) sea level anomaly (SLA) field available from Copernicus Marine Environment Monitoring Service (CMEMS) (http://marine.copernicus.eu). SLA values were selected for 8 grid points, which we label A_1 to A_8, along 6.125°W from 62.125°N to 63.875°N (Figure 1b). For each of these points, we have sea level anomalies $H_k(t)$, $k = 1$ to 8, for 9292 days from 1 January 1993 to 10 June 2018.

In addition to ADCPs and altimetry, information on the velocity structure may be gained from baroclinic velocity profiles derived from CTD data along the section assuming geostrophy. Between 1990 and 2018, there have been more than one hundred CTD cruises with occupations of the standard stations on the section (Figure 1). A baroclinic profile requires CTD data from two neighbouring stations and good data were not always recovered from all of the stations, but the CTD data still provided more than a hundred baroclinic profiles from all of the station pairs, although only just below one hundred of them were within the altimetry period (after 1 Jan 1993) for most of the pairs.

3 Calibrating altimetry data to give eastward surface velocities

At time scales exceeding a few days, we expect approximate geostrophic balance, so that the horizontally averaged eastward surface ($z = 0$) velocity $U_k(0,t)$ between grid points A_k and A_{k+1} is proportional to the difference in absolute sea level height (SLH) between the two points. The SLA values, $H_k(t)$, do not represent absolute SLH (above the geoid), but rather the anomaly. Surface velocities derived from SLA differences between two grid points are therefore also anomalies, but may be made absolute by adding a constant ***"Altimetric offset"*** U_k^0 for each interval:

$$U_k(0,t) = \frac{g}{f \cdot L} \cdot [H_k(t) - H_{k+1}(t)] + U_k^0 = \frac{g}{f \cdot L} \cdot \Delta H_k(t) + U_k^0 \qquad (1)$$

where g and f are gravity and Coriolis parameter, respectively, and L is the distance between the altimetry grid points and we have defined: $\Delta H_k(t) \equiv [H_k(t) - H_{k+1}(t)]$. Calibrating the altimetry data means determination of the constants U_k^0 for each altimetry interval. In H2015 this was done for the region between altimetry points A_2 and A_8 based on the available ADCP data and average baroclinic profiles that were derived from the CTD data (H2015 Figure 5 and Table S2.4.4[1]).

At that time there were, however, no ADCP data acquired south of point A_3 or north of point A_6. This was the reason for adding two new ADCP sites, NI located in interval A_2 to A_3 and NH located in interval A_6 to A_7 (Figure 1b). Also, new data have been acquired both from additional ADCP deployments at the long-term sites and additional CTD cruises. Our first task (Task 1) is therefore to check and update Table S2.4.4 in H2015. Before that, the ADCP data must, however, be extrapolated to the surface.

3.1 Extrapolation of ADCP velocities towards the surface

Upward-looking ADCPs do not reach all the way to the surface (Table 2) and the velocity profiles therefore have to be extrapolated over the last depth interval to get surface velocity. The procedure for doing that is based on the observed fact that temporal velocity variations at different depths on the N-section are highly correlated (barotropic) as long as the difference in depth is not too high (Figure 2). To a first approximation, this implies that the velocities at various depths are proportional to one another, which may be used to extrapolate the eastward velocity from the uppermost measurement to the surface.

To implement this, assume that the ADCP data on a specific day, t, are error-free up to a depth z_t. The eastward velocity $U(z,t)$ may then be estimated for all depths $z < z_t$ by using:

$$U(z,t) = \frac{\alpha_0(z)}{\alpha_0(z_t)} \cdot U(z_t,t) \qquad (2)$$

where $\alpha_0(z)$ is a time-independent function of depth for each ADCP site. This ***extrapolation factor*** may be evaluated iteratively in one meter steps (from $z + 1$m to z) by a regression analysis requiring zero-offset using all days with good measurements at both z and $z + 1$m.

$$\alpha_0(z) = \alpha_0(z+1) \cdot \frac{\sum_t U(z,t) \cdot U(z+1,t)}{\sum_t U(z+1,t) \cdot U(z+1,t)} \qquad (3)$$

with $\alpha_0(z_{Min}) = 1$, where z_{Min} is the shallowest depth with complete ADCP coverage (Table 2). This method may be used to estimate $\alpha_0(z)$ up to the shallowest level, z_{Ext}, reached by the ADCP at the site. As seen in Figure 2, the number of days decreases rapidly, as we approach this level, but most of the sites still have more than 200 days of observation, as indicated in the last row of Table 2.

---

[1] For references to the Supplementary document associated with H2015, we add an "S" to the figure, table, and equation numbers.

Table 2. Depth of the bottom (Bott.), of the deepest (z_{Max}), and of the shallowest (z_{Min}) level with complete ADCP coverage. The last two rows list the depth of the shallowest level (z_{Ext}) with ADCP data at the site and the number of days with measurements at this depth.

Site:	NI	NA	NE	NF	NB	ND	NG	NC	NH
Bott.:	156m	300m	455m	700m	925m	1280m	1815m	1730m	1802m
z_{Max}:	139m	275m	418m	600m	600m	600m	588m	586m	600m
z_{Min}:	79m	151m	174m	203m	262m	209m	229m	198m	135m
z_{Ext}:	39m	35m	73m	78m	72m	84m	63m	61m	65m
Days:	329	210	303	258	304	177	314	89	332
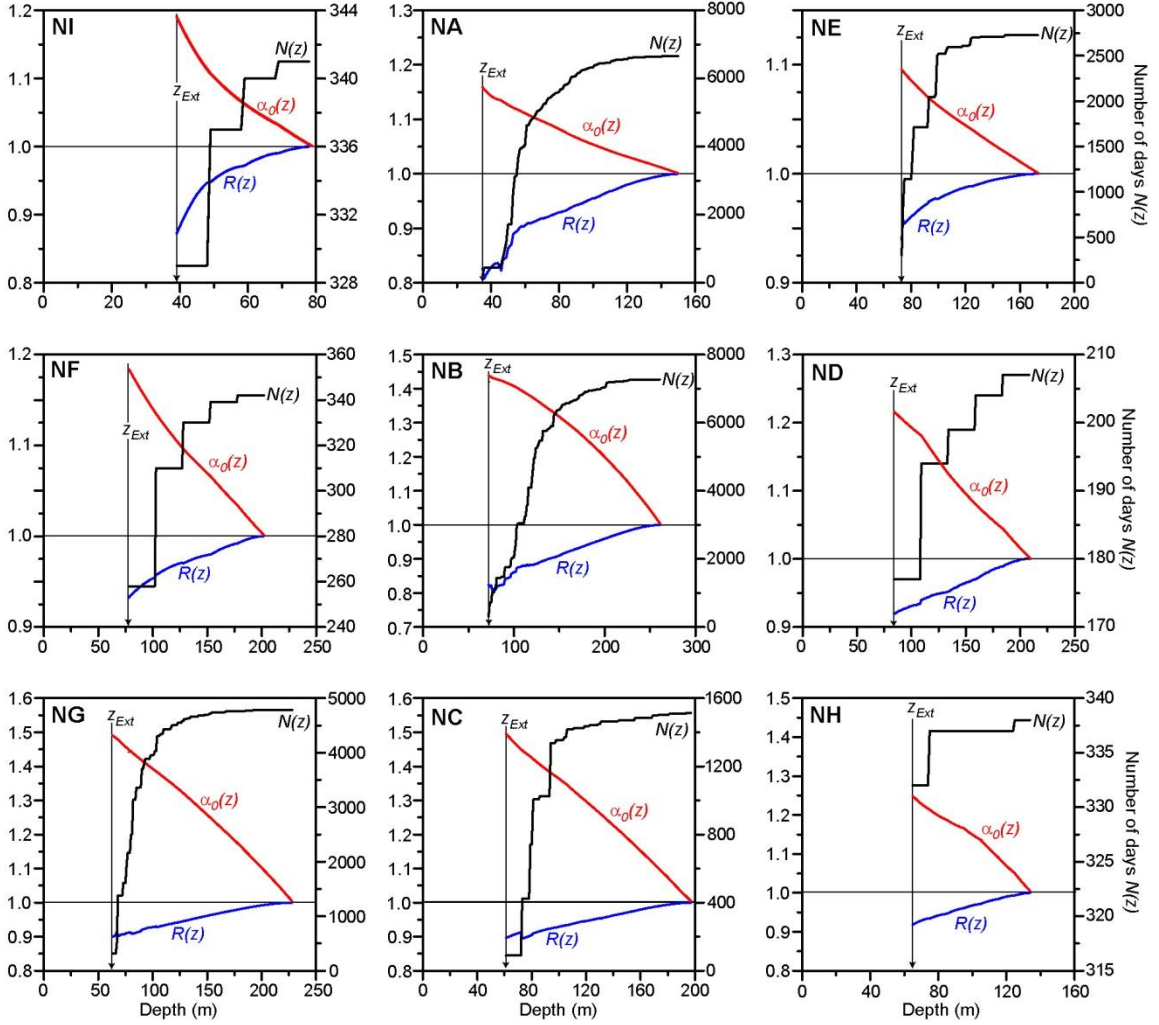
Figure 2. Vertical variation of eastward velocity close to the surface for the nine ADCP sites. Each panel shows the number of days with data at each depth, $N(z)$ (black curve, right scale), the correlation coefficient between $U(z,t)$ and $U(z_{Min},t)$, $R(z)$ (blue curve, left scale), and the extrapolation factor $\alpha_0(z)$ as determined by Eq. (3) (red curve, left scale). Here, $U(z,t)$ is eastward velocity at depth z for time t and z_{Min} is the depth, up to which all profiles from the site were complete.

3.2 Seasonally varying extrapolation

Although Eq. (2) with a time-independent extrapolation factor $\alpha_0(z)$ generally is a good approximation, it may be improved by taking seasonal variation into account. The seasonal variation of the velocity profile is perhaps most pronounced for the two southernmost (and shallow) sites, but is also clear for other sites (Figure 3).
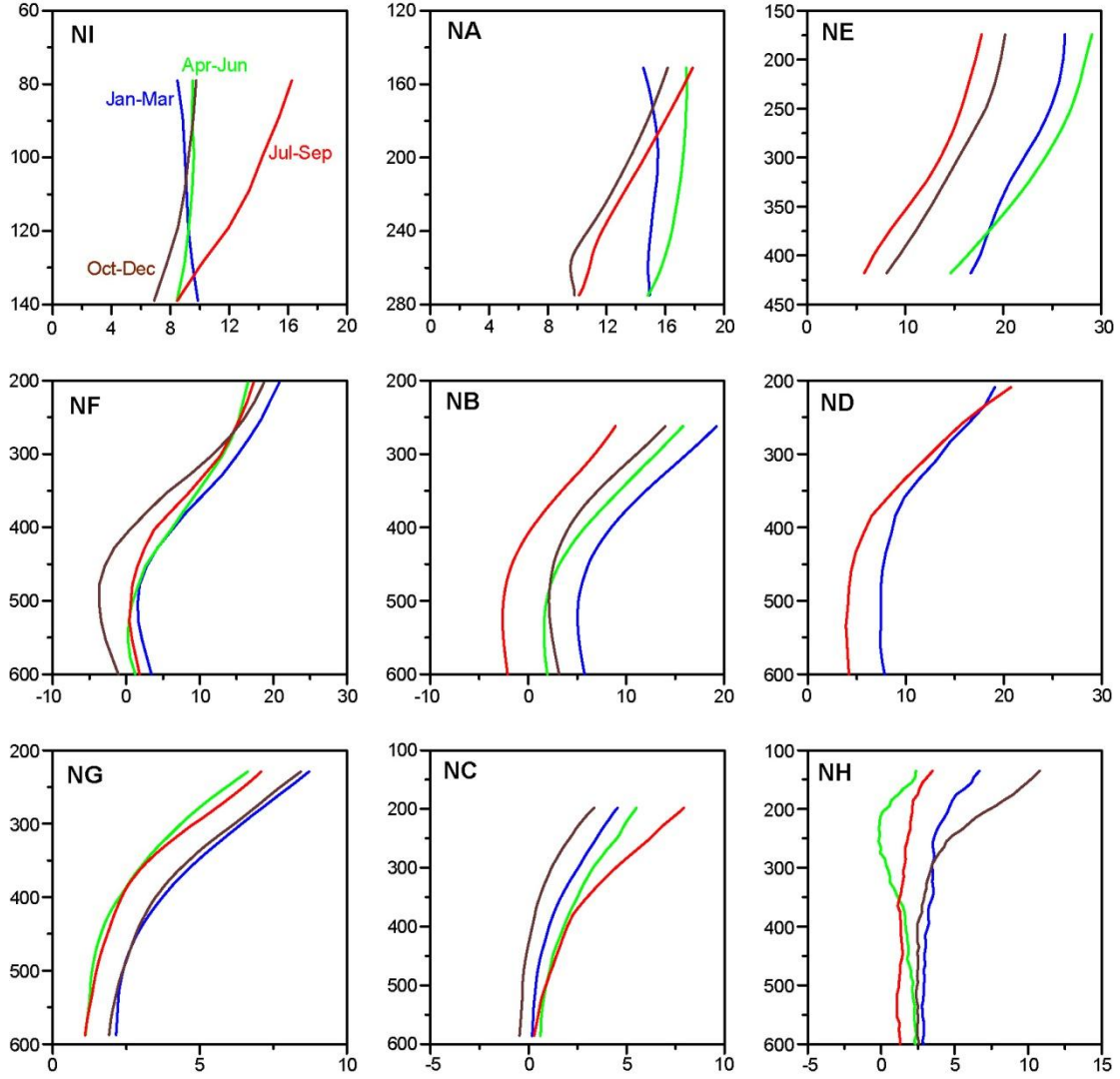
Figure 3. Vertical variation of eastward velocity between z_{Min} and z_{Max} averaged for each of the four seasons separately as indicated in the top left panel: January to March (blue), April to June (green), July to September (red), and October to December (brown).

To account for this, extrapolation factors have been calculated for individual months separately for each of the sites, except site NF and ND[2]. This was done by running the calculations in Eq. (3) for each of the twelve months of the year where only observations from the selected month and the two neighbouring months are included in the sums in Eq. (3). For each of these sites, this analysis produces twelve extrapolation factors $\alpha_m(z)$ ($m = 1, ..., 12$). All of these factors are 1 for $z = z_{Min}$, but the seasonal character strengthens as we approach the surface.

For most of the sites, the top values of the extrapolation factor, $\alpha_m(z_{Ext})$, show a consistent seasonal variation (Figure 4) that may be approximated by a sinusoidal function:

$$\alpha_m(z_{Ext}) \cong \alpha_0(z_{Ext}) \cdot \left[1 + \alpha_s \cdot \cos\left(\frac{2\pi}{12} \cdot (m - M)\right)\right] \qquad (4)$$

where m is the number of the month considered and M is the number of the month with maximum value for $\alpha_m(z_{Ext})$. The parameter α_s indicates the strength of the seasonal variation. To determine these parameters for each site, the twelve monthly values of $\alpha_m(z_{Ext})$ were regressed on the cosine function

---

[2] These two sites have short data records, are close to the long-term site NB, and do not contribute additional useful information. They will not be used further in the analysis.

in Eq. (4), varying the value of M to give maximum correlation, R_{Max}. As shown in Table 3, all the sites except NE and NH had fairly high values for R_{Max}, indicating good fits. At site NE, the extrapolation factor does not appear to have any significant seasonal variation, which is consistent with Figure 3 where the average eastward velocity at this site does not change much with depth in the top layer. The change in parameter values from one site to the next also indicates consistency. The two southernmost sites, NI and NA, both have maximum values for $\alpha_m(z_{Ext})$ in November and similar values for α_s. At site NB, the maximum occurs in June and at sites NG and NC, it has moved to March-February.

Table 3. Maximum correlation coefficient, R_{Max}, and parameters in Eq. (4) from regression analysis.

Site:	NI	NA	NE	NB	NG	NC	NH
R_{Max}:	0.93	0.97	0.58	0.94	0.82	0.87	0.75
M:	11	11	5	6	4	2	5
α_s:	0.11	0.08	0.01	0.09	0.07	0.11	0.09
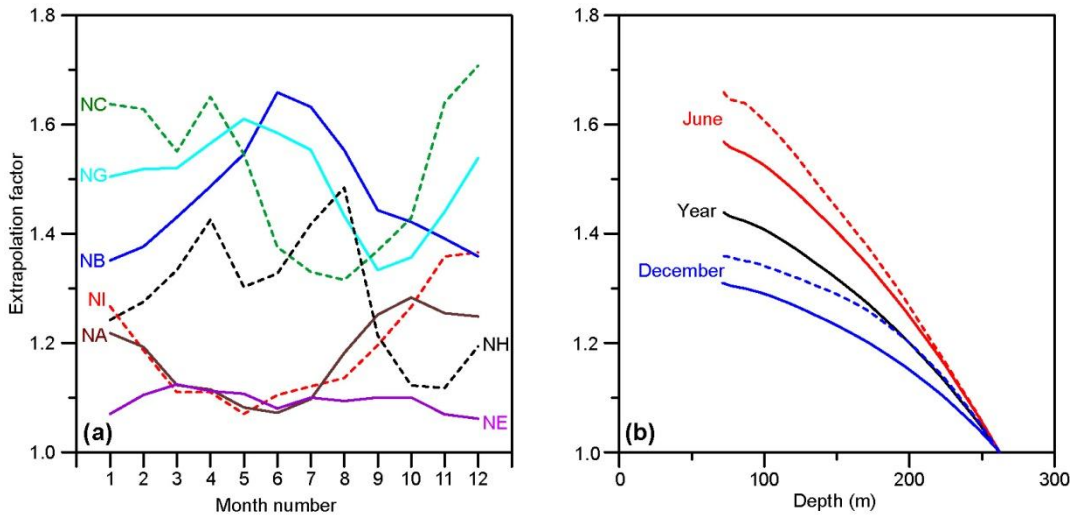
Figure 4. **(a)** Seasonal variation of the top values for the extrapolation factors, $\alpha_m(z_{Ext})$, based on overlapping 3-month periods for all the ADCP sites except NF and ND. Continuous lines indicate the four long-term sites. **(b)** Depth variation of the extrapolation factors for site NB for the whole year (black), $\alpha_0(z)$, for December (blue), $\alpha_{12}(z)$, and for June (red), $\alpha_6(z)$. Dashed red and blue curves represent the original values for $\alpha_{12}(z)$, and $\alpha_6(z)$. Continuous red and blue curves are based on the approximation in Eq. (5) with the parameters in Table 3.

When implementing a seasonally varying extrapolation factor, we can either choose to use the original values, $\alpha_m(z)$, determined for each month, or we may choose to use a factor that varies sinusoidally with season. Equation (4) only applies to the level z_{Ext}, but it may be extended to other depths with the approximation:

$$\alpha_m(z) \cong \alpha_0(z) \cdot \left[1 + \alpha_s \cdot \frac{\alpha_0(z)-1}{\alpha_0(z_{Ext})-1} \cdot \cos\left(\frac{2\pi}{12} \cdot (m - M)\right) \right] \qquad (5)$$

which reduces to Eq. (4) at $z = z_{Ext}$ and to $\alpha_m(z) = \alpha_0(z) = 1$ for $z = z_{Min}$. The difference between these two choices is illustrated in Figure 4b for site NB. A priori, it might seem most appropriate to use the original values for each month but for the sites with few deployments (especially NI and NH), the original values for $\alpha_m(z)$ are only based on few observations and even the best observed sites have fewer observations in summer during the annual servicing periods (Table A1). This is illustrated in Figure 4 for site NB, which is seen on Figure 4a to have an extreme value for $\alpha_m(z_{Ext})$ in June, when there are fewer observations than in most other months. We therefore choose to use Eq. (5) with the values in Table 3.

3.3 Near-surface extrapolation based on CTD data

Having extrapolated the ADCP velocities up to the level z_{Ext}, other data sources are needed to extrapolate all the way to the surface. In H2015, this was done by using the CTD observation along the section to calculate baroclinic velocity profiles from the density structure. This structure is illustrated in the top and middle panels in Figure 5, where we have chosen one standard station in the southern end of the section (N02), one station close to the northern boundary of the Atlantic domain (N08), and one in the middle (N05).

As demonstrated in the figure, there are a large number of observations that cover most of the year, but with few profiles from December and January. From the top panels in Figure 5, the southernmost (and shallow) region (around N02) never becomes highly stratified but farther north (around N05 and N08); the top 100 m become stratified in summer, although to a highly variable degree.
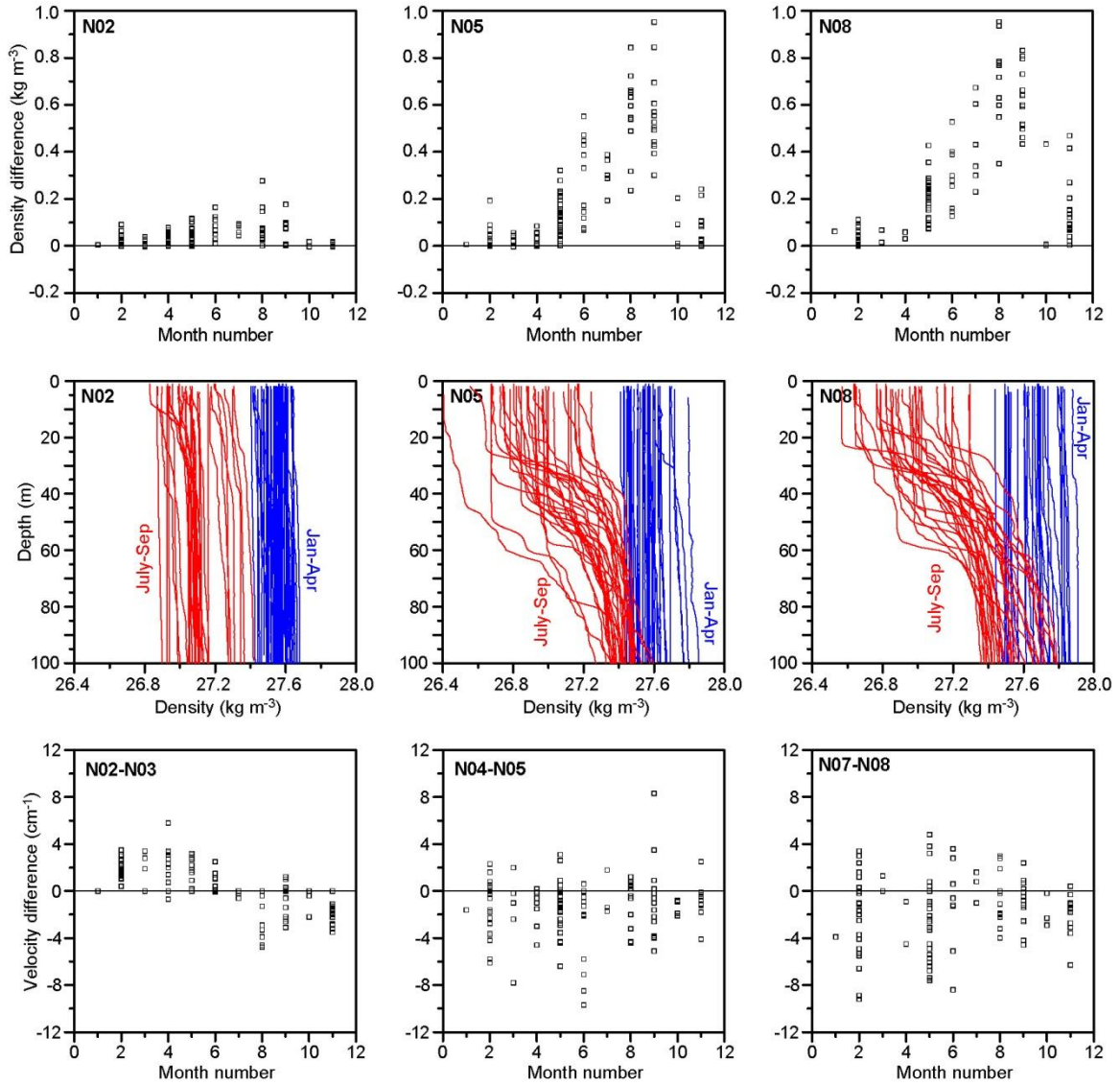
Figure 5. Seasonal variations in density and baroclinic velocity in the top 100 m in three different regions of the N-section based on CTD data. **Top panels:** Density difference (σ_θ) between the surface and 100 m depth in different months. Each square is from one CTD profile. **Middle panels:** Density profiles (σ_θ) in July-September (red) and in January-April (blue). **Bottom panels:** Difference in eastward velocity between the surface and 100 m depth based on geostrophic calculations from CTD data.

Throughout most of the year, there are periods with no or only limited stratification in the upper 100 m, but in the three months from July to September, the northern part of the section seems to be consistently stratified close to the surface. As demonstrated in the middle panels of Figure 5, the density structure is, however, also very variable during this period (red profiles).

On every cruise when CTD observations have been carried out quasi-simultaneously at two neighbouring standard stations, we can use the traditional dynamical method to calculate the vertical variation of the eastward velocity between the two stations. From the bottom panels in Figure 5, the velocity difference between the surface and 100 m depth may approach 10 cm s^{-1}, but is highly variable. Only in the southernmost part of the section (station N02) does there seem to be a consistent seasonal variation, which is verified in Figure 6.
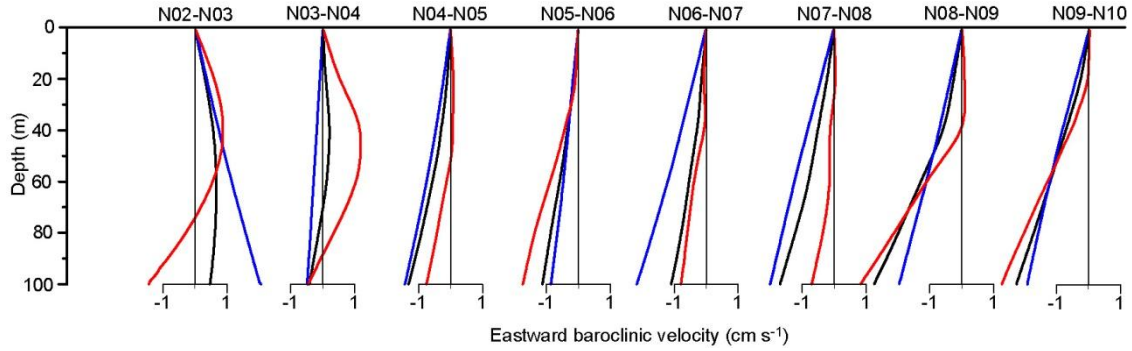
Figure 6. Vertical variation of the eastward baroclinic velocity between each pair of neighbouring standard section from N02 to N10 based on dynamic calculation of CTD observations. Black profiles are averages for the whole year. Red profiles are for the July-September period and blue profiles are for the January-April period. All the profiles are set to zero velocity in the surface.

In order to use the information from the baroclinic velocity profiles, we make the assumption that the temporally averaged baroclinic velocity profile in the top layer can be used as an extension of the average ADCP velocity profile:

$$\alpha_0(z) = \alpha_0(z_{Ext}) \cdot \frac{\langle U(z_{Ext})\rangle + \langle U_{Bc}(z)\rangle - \langle U_{Bc}(z_{Ext})\rangle}{\langle U(z_{Ext})\rangle} \qquad (6)$$

where $U(z_{Ext})$ is the ADCP velocity at the uppermost observed level, $U_{Bc}(z)$ is the baroclinic velocity at depth z, and $\langle\ \rangle$ indicates temporal averaging. Ideally, this should be done for individual months or seasons separately, but the available data set is not sufficiently comprehensive and consistent to allow that. We therefore use the annually averaged baroclinic velocity profiles in Eq. (6) for all the ADCP sites.

With this final step, the velocity profiles from the seven selected ADCP sites have been extrapolated all the way to the surface and Figure 7 illustrates the full, vertically extrapolated eastward velocity profiles at these sites by showing the average profiles as well as their standard deviations. Figure 7 also shows average baroclinic velocity profiles, based on CTD observations at pairs of standard stations (Figure 1) that straddle the ADCP sites and adjusted so that they show the same velocity as the average ADCP velocity at its deepest level.

When comparing the ADCP-based (black) and the baroclinic CTD-based (red) average profiles in Figure 7, we have to take into account that they are averaged over different periods of time, which is especially important for the sites with only one deployment (NI and NH). Also, the ADCP-based profiles are from one location whereas the CTD-based profiles are horizontally averaged over the interval between the two CTD standard stations in each pair. With that in mind, the correspondence between the two sets of average profiles is fairly good.
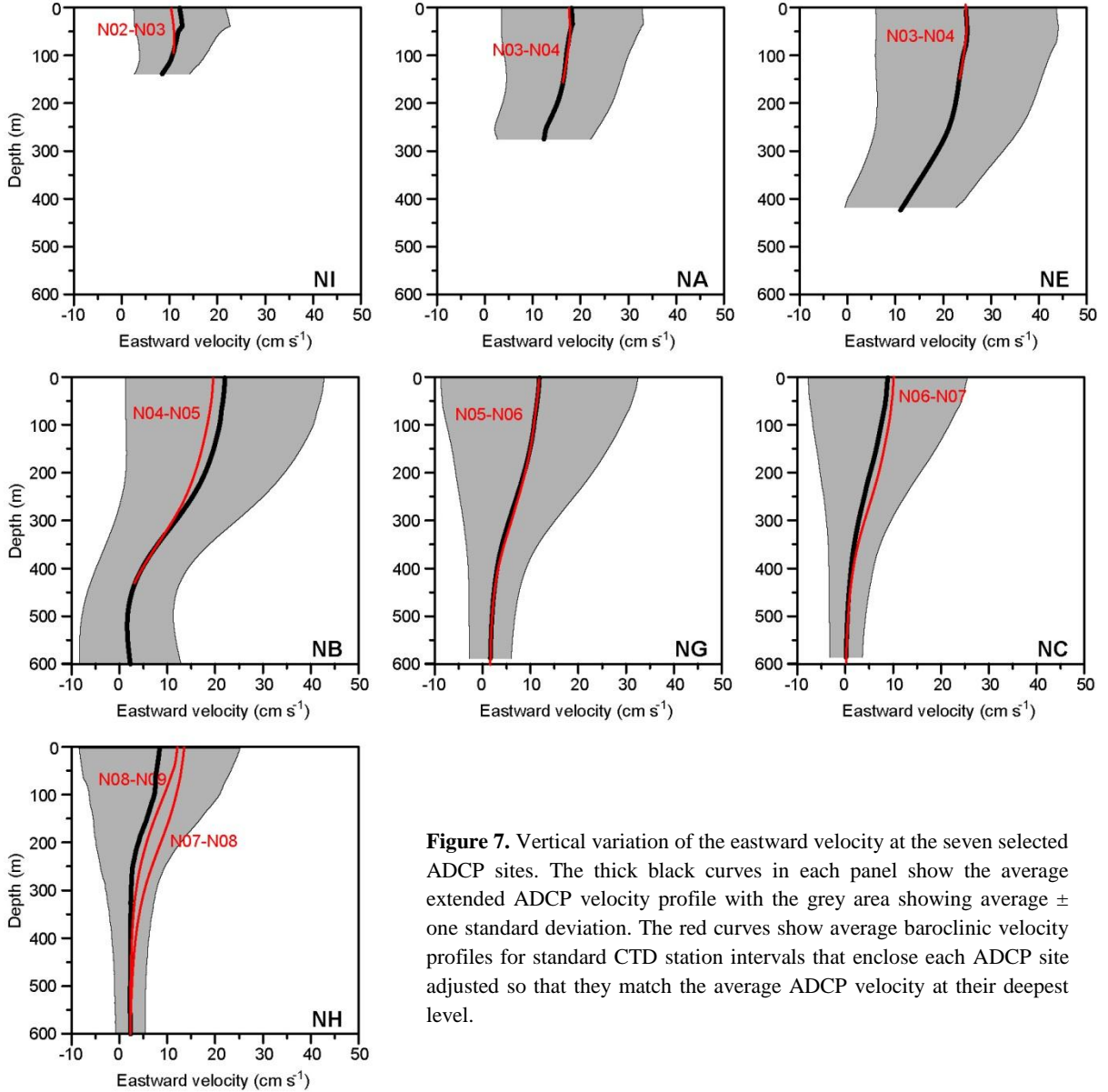
Figure 7. Vertical variation of the eastward velocity at the seven selected ADCP sites. The thick black curves in each panel show the average extended ADCP velocity profile with the grey area showing average ± one standard deviation. The red curves show average baroclinic velocity profiles for standard CTD station intervals that enclose each ADCP site adjusted so that they match the average ADCP velocity at their deepest level.

3.4 Linking ADCP velocities and altimetry data

As long as the assumption of geostrophy is valid, one might perhaps expect high correlations between surface velocities based on ADCP data and anomalies of sea level slope across the interval between two altimetry points that straddle the ADCP sites consistent with Eq. (1). Indeed, there are indications of this, but not overwhelmingly so even if we average over 28 days before correlating[3] (Table 4).

Certainly, there are some fairly high and highly significant correlation coefficients in Table 4, but they are not all high and only for sites NE and NB do the correlations explain more than 50% of the variance. It has to be kept in mind, however, that an ADCP measures the velocity profile at one location whereas the sea level difference between two altimetry points depends on the horizontally averaged surface velocity between the two points even with perfect geostrophy. To get a high positive correlation in Table 4, the ADCP-derived surface velocity has to represent the whole region between the two altimetry points straddling it and that is not generally the case as demonstrated in Table 5.

---

[3] Most ADCP deployments have lasted at least 336 days, which assures that at least 12 non-overlapping 28-day averaged velocity profiles are available from each deployment (12×28=336).

Table 4a. Correlation coefficients[4] between 28-day averaged values for eastward surface velocities from ADCPs and differences in SLA values between two neighbouring points. Correlation coefficients are bold and underlined when the ADCP site is within the interval between the two altimetry points. If the site is close to one of the points, the closest neighbouring interval is also shown in bold (but not underlined). The second column (N) indicates the number of 28-day periods used for calculation of each correlation coefficient.

Site	N	A_1–A_2	A_2–A_3	A_3–A_4	A_4–A_5	A_5–A_6	A_6–A_7	A_7–A_8
NI	12	0.34	**0.42**	-0.11	-0.17	0.14	0.18	0.03
NA	231	0.16	**0.62*****	**0.28*****	-0.18	-0.45***	-0.20**	0.06
NE	95	-0.23	0.51***	**0.78*****	0.36*	-0.31*	-0.53***	-0.27*
NB	253	-0.29**	0.17*	**0.76*****	**0.73*****	0.08	-0.60***	-0.55***
NG	167	-0.16	-0.46***	0.05	**0.61*****	0.67***	-0.12	-0.46***
NC	53	-0.06	-0.30*	-0.24	-0.01	**0.39****	0.35**	0.02
NH	12	0.33	0.07	-0.19	-0.20	0.25	**0.65***	0.36

Table 4b. Correlation and regression coefficients between 28-day averaged values for eastward surface velocities from ADCPs and differences in SLA values between the two neighbouring altimetry points that straddle the ADCP location. The last two columns list the coefficients in the regression equation $U(0,t) = a \cdot \Delta H(t) + b$ with 95% confidence intervals.

Site	Altimetry	Correl.	a (s^{-1})	b (cm s^{-1})
NI	A_2–A_3	0.42	2.4 ± 3.8	12.4 ± 3.0
NA	A_3–A_4	0.28***	1.2 ± 0.6	18.2 ± 1.0
NE	A_3–A_4	0.78***	5.0 ± 0.8	24.3 ± 1.4
NB	A_4–A_5	0.73***	4.3 ± 0.5	22.7 ± 1.1
NG	A_4–A_5	0.61***	3.1 ± 0.6	12.6 ± 1.3
NC	A_5–A_6	0.39**	2.1 ± 1.4	8.6 ± 1.9
NH	A_6–A_7	0.65*	5.7 ± 4.7	10.1 ± 5.0

The correlation coefficients are generally lower in Table 5 than in Table 4. The distance between two neighbouring altimetry points is more than 27 km and Table 4 clearly indicates that surface velocities at two points on the section within that distance from one another do not in general have high positive correlations. One could speculate that this was due to the vertical extrapolation associated with using Eq. (2), but recalculating the correlation coefficients at a depth of z_{Min} or deeper did not give substantially better correlations except for the correlation between velocity at NA and NE, which seems to increase with depth (from R = 0.59*** at 175 m depth to R = 0.67*** at 275 m depth).

Table 5. Correlation coefficients between 28-day averaged values for eastward surface velocities at two different ADCP sites that have been measured in overlapping periods.

Site	NE	NB	NG	NC	NH
NI		-0.38			
NA	0.34*	-0.10	-0.40***	-0.01	
NE		0.64***	-0.32**		
NB			0.17*	-0.26	0.00

In Table 4a, we also note that the surface velocities from the ADCPs in several cases (for NA, NB, and NG) are better correlated with SLA differences across a neighbouring altimetry interval than the interval that they are located in. Thus, the lack of correlation coefficients close to 1 in Table 4 does not necessarily imply that surface velocities derived from altimetry are not realistic. Rather, we conclude from Table 4 that ADCPs (or other in situ current measuring instruments) need to be located close to one another to ensure coherent velocity profiles. Covering the whole section with a sufficient number of ADCPs to ensure accurate transport estimates would therefore require a huge investment in instrumentation and manpower.

Both Table 4 and Table 5 also exhibit highly significant negative correlation coefficients, which may derive from mesoscale features passing through the section or from north-south shifts of the

---

[4] Here and elsewhere statistical significance is indicated by asterisks: "*" indicates p<0.05, "**" indicates p<0.01, "***" indicates p<0.001. Significance levels are corrected for serial correlation using the "Modified Chelton method" (Pyper and Peterman, 1998).

velocity field. Since altimetry integrates surface velocity, it will be less sensitive to such shifts than in situ instrumentation, as long as geostrophy is valid.

These results, thus, support the strategy adopted in H2015, that variations in surface velocity are best derived from altimetry, at least on monthly timescales. As demonstrated in H2015, the Mean Dynamic Topography is, however, too smooth to give reliable absolute surface velocities and we have to rely on in situ measurements to give appropriate values for the U_k^0 constants in Eq. (1). In H2015, the method for using ADCP velocities to estimate U_k^0 in altimetry interval A_k–A_{k+1} was based on converting Eq. (1) into Eq. (7):

$$U_k^0 = \langle U_k(0,t) - \frac{g}{f \cdot L} \cdot \Delta H_k(t) \rangle \qquad (7)$$

where $\langle \ \rangle$ indicates temporal averaging. For each ADCP site, we use daily averaged eastward surface velocity from the extended ADCP profiles to represent $U_k(0,t)$ and simultaneous SLA values to represent the difference in sea level across the altimetry interval containing the ADCP site, $\Delta H_k(t)$. Resulting values for U_k^0 are listed with confidence intervals in the bottom row of Table 6:

Table 6. Characteristics of eastward surface velocities at the nine ADCP sites as well as values for U_k^0 and their 95% confidence intervals[5] determined from the ADCP sites within each altimetry interval. The lowest three rows are in cm s^{-1}.

Interval:	A_2–A_3	A_3–A_4		A_4–A_5		A_5–A_6	A_6–A_7
ADCP site:	NI	NA	NE	NB	NG	NC	NH
Days:	342	6663	2729	7272	4788	1517	339
Average:	12.1	18.1	24.8	22.2	11.9	8.8	8.3
Std.dev.:	9.6	14.7	18.9	20.8	20.7	16.6	16.8
U_k^0:	12.5±2.3	18.4±2.0	24.6±1.8	22.6±2.1	12.4±1.6	8.2±2.3	9.2±4.9

In H2015, this method was used for the sites NA and NE to give two separate estimates of U_3^0 for altimetry intervals A_3-A_4. Similarly, ADCP velocities from sites NB and NG were used to give two estimates of U_4^0 for interval A_4-A_5. These values (H2015 Table S2.4.1) equal the values in Table 6 within the confidence intervals. The two different estimates of U_k^0 may then be combined to give a resulting estimate for each of the intervals as illustrated by Figure S2.4.4 in H2015.

For these two altimetry intervals, one may alternatively combine the surface velocities from the two ADCP sites in each interval before averaging. Thus, we assume that the eastward surface velocity, horizontally averaged within interval A_4-A_5 may be expressed as a linear combination of the surface velocities from ADCP sites NB and NG:

$$U_4(0,t) = \beta_{NB} \cdot U_{NB}(0,t) + \beta_{NG} \cdot U_{NG}(0,t) \qquad (8)$$

where we require that $\beta_{NB} + \beta_{NG} = 1$ to indicate that the ADCPs at NB and NG each represent a fraction of the altimetry interval. To determine the optimal combination, we use a "least squares" approach, minimizing the sum:

$$S = \sum_t \left\{ U_4(0,t) - \frac{g}{f \cdot L} \cdot \Delta H_4(t) - U_4^0 \right\}^2 \qquad (9)$$

where U_4^0 for each combination is determined by Eq. (8). From Figure 1b, one might expect the two ADCPs to represent similar fractions of the interval and, indeed, it is found that the combination $\beta_{NB} = 0.51$ and $\beta_{NG} = 0.49$ minimizes the sum in Eq. (9). For this combination, the result was:

$$U_4^0 = (17.4 \pm 0.9) \, \text{cm s}^{-1} \qquad (10)$$

---

[5]Here and elsewhere, the 95% confidence intervals are the standard errors multiplied by 1.96, corrected for serial correlation by replacing the sample size by the "equivalent sample size" (von Storch, 1999) calculated from the autocorrelation of the time series.

This average is almost identical to the average of the two values for NB and NG in Table 6, but the uncertainty in Eq. (10) is considerably lower than would be obtained from combining the uncertainties in Table 6. To check the validity of this approach, we have generated a series of 28-day averaged values (166 values) for $U_4(0,t)$ using the determined values of β_{NB} and β_{NG} and the corresponding series of 28-day averaged values for $\Delta H_4(t)$. The correlation coefficient between these two series was $R_{28} = 0.89^{***}$, which is substantially higher than the correlation coefficients for this interval in Table 4. A linear regression analysis gave the relationship:

$$U_4(0,t) = G_{Reg4-5} \cdot \Delta H_4(t) + U_4^0 \qquad (11a)$$

with:

$$G_{Reg4-5} = (3.69 \pm 0.30)\,\text{s}^{-1} \quad \text{and} \quad U_4^0 = (17.6 \pm 0.7)\,\text{cm s}^{-1} \qquad (11b)$$

The values for U_4^0 in Eq. (11b) and Eq. (10) are quite consistent, but the value for G_{Reg4-5} is considerably higher than the theoretical value (with $g = 9.82$ m s^{-2}, $f = 1.296 \cdot 10^{-4}$ s^{-1}, $L = 27.9$ km):

$$G_{Theory} = \frac{g}{f \cdot L} = 2.72\,\text{s}^{-1} \qquad (12)$$

Similarly, we may represent the average velocity of altimetry interval A$_3$-A$_4$ as a linear combination of the surface velocities from the two ADCPs, NA and NE, in that interval, but site NB is also close to this interval and was well correlated with it (Table 4a). We therefore include the surface velocity from this site into the combination:

$$U_3(0,t) = \gamma_{NA} \cdot U_{NA}(0,t) + \gamma_{NE} \cdot U_{NE}(0,t) + \gamma_{NB} \cdot U_{NB}(0,t) \qquad (13)$$

with $\gamma_{NA} + \gamma_{NE} + \gamma_{NB} = 1$. Using a least squares approach determined the optimal combination to be for $\gamma_{NA} = 0.31$, $\gamma_{NE} = 0.32$, and $\gamma_{NB} = 0.37$. For 28-day averaged data, the correlation with $(H_3(t) - H_4(t))$ was $R_{28} = 0.82^{***}$ and the Altimetric offset:

$$U_3^0 = (21.6 \pm 1.1)\,\text{cm s}^{-1} \qquad (14)$$

A linear regression analysis analogous to Eq. (11a) gave the result:

$$G_{Reg3-4} = (3.69 \pm 0.53)\,\text{s}^{-1} \quad \text{and} \quad U_3^0 = (21.4 \pm 0.9)\,\text{cm s}^{-1} \qquad (15)$$

According to H2015 (Figure S5.4.1), around three quarters of the Atlantic water transport through the section passes between altimetry points A$_3$ and A$_5$. It may therefore be worthwhile to assess, how well altimetry can represent the average eastward surface velocity in the interval between these two points. If we assume that Eq. (8) and Eq. (13) with the estimated values for the β and γ weighting factors do represent realistic velocities, horizontally averaged over each of the altimetry intervals, then the average surface velocity between A$_3$ and A$_5$, as determined by ADCP measurements, is:

$$U_{3-5}(0,t) = \tfrac{1}{2} \cdot [0.31 \cdot U_{NA}(0,t) + 0.32 \cdot U_{NE}(0,t) + 0.88 \cdot U_{NB}(0,t) + 0.49 \cdot U_{NG}(0,t)] \qquad (16)$$

This horizontally averaged velocity may be calculated for all days with simultaneous ADCP measurements at all four sites, which is a total of 2706 days. When averages are calculated for each of the 94 contiguous 28-day sequences in the time series and correlated with 28-day averaged SLA difference between A$_3$ and A$_5$, the correlation coefficient is found to be $R_{28} = 0.86^{***}$. Since altimetry data have been used to derive the weighting factors in Eq. (16), the two time series are not totally independent, but this value for R_{28} remains significantly different from zero at the $p < 0.001$ level even after reducing the degrees of freedom (which were already corrected for serial correlation) accordingly. A linear regression analysis analogous to Eq. (11a) gave the result:

$$G_{Reg3-5} = (1.72 \pm 0.21)\,\text{s}^{-1} \quad \text{and} \quad \tfrac{1}{2}(U_3^0 + U_4^0) = (19.5 \pm 0.7)\,\text{cm s}^{-1} \qquad (17)$$

The second of these two values is the same as would be obtained by averaging Eq. (10) and Eq. (14) although the uncertainty is smaller. Since the distance L in Eq. (12) in this case is twice as long, the theoretical value for G_{Theory} is only 1.36 s^{-1} and the value for G_{Reg3-5} in Eq. (16) is 26% higher than required by theory. This is also illustrated in Figure 8 where we see that the velocity based on extrapolated ADCP data using Eq. (16) varies more than the velocity based on altimetry with the theoretical value $G_{Theory} = 1.36$ s^{-1}.
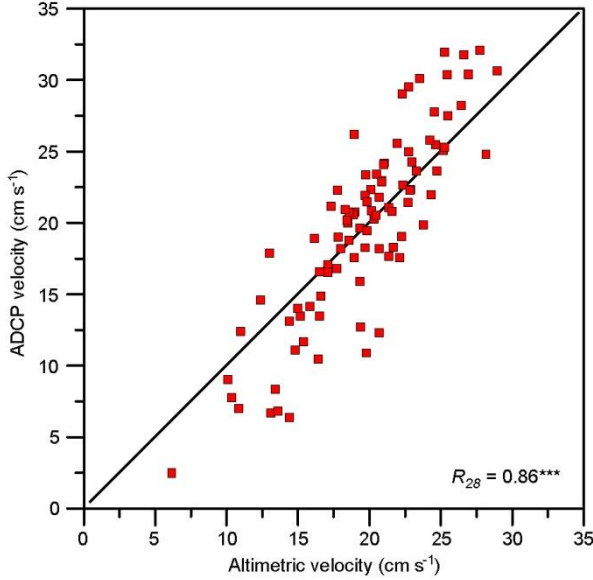
Figure 8. Comparing two different estimates of eastward surface velocity horizontally averaged between altimetry points A_3 and A_5. Each square represents a 28-day average with the value based on altimetry along the abscissa and the value based on ADCP measurements, Eq. (16), along the ordinate. The diagonal line indicates equality.

A priori, the high value for G_{Reg3-5} compared to theory and the deviation from 1 in the slope of the squares in Figure 8 are discouraging. We note, however, that the deviation from theory in Eq. (17), 26%, is less than in Eq. (11b) and Eq. (15), 36%, which again is less than the deviations in Table 4b for the two best correlated ADCP sites, NE (84%) and NB (58%). As illustrated in Figure 9, this kind of deviation from theory is to be expected when the core of a current can move back and forth laterally. The case in this figure is extreme and not very representative for the N-section, but the general argument – that with limited spatial resolution of the ADCP array, deviations are likely – remains. The deviation of the regression factor from theory is therefore to be expected and is not a reason for questioning the theoretical value in Eq. (12).
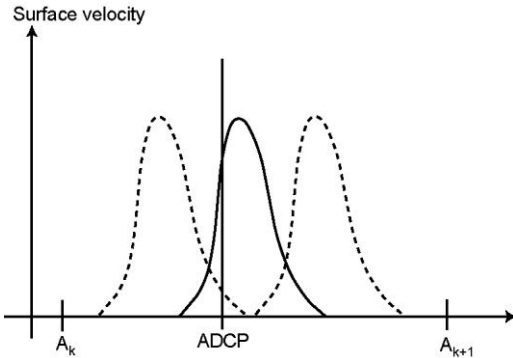
Figure 9. A hypothetical (extreme) situation with a narrow current that remains constant in shape, but moves back and forth past a location with an ADCP. Since the current is assumed to stay within the interval between two altimetry points A_k and A_{k+1}, the horizontally averaged surface velocity between these two points remains constant and an altimetry-derived surface velocity would also be constant. The extrapolated surface current from the ADCP would, however, vary between zero and the maximum velocity in the current core.

If we could assume that the ADCP velocity generated by Eq. (16) was a perfect representation of the average eastward surface velocity between A_3 and A_5, then the high correlation coefficient would imply that the velocity generated from altimetry data by using Eq. (1) could explain 74% (0.86^2) of

the variance in the real velocity on monthly time scales. In reality, the uncertainties involved in vertical extrapolation and insufficient horizontal resolution of the ADCP array (Table 5) imply that Eq. (16) cannot be a perfect representation of reality. Some of the "noise" in the relationship between Altimetric velocity and ADCP velocity must derive from this uncertainty, which further implies that the 74% are probably an underestimate.

Thus, we conclude that *the velocity generated from altimetry data after calibration by in situ ADCPs probably explains more than 74% of the variance in the real surface velocity horizontally averaged between A_3 and A_5 on monthly time scales*. For other parts of the section, we don't have a similar amount of in situ data to check the validity of altimetry, but there does not appear to be any good reason why it should perform much worse.

We therefore also conclude that *the adopted monitoring strategy, which is based on estimating surface velocity from altimetry data, calibrated by in situ measurements, is solidly based*.

3.5 Linking baroclinic velocity from CTD cruises with altimetry

When we have quasi-synoptic (within a day) CTD data from two CTD standard stations, we can calculate the velocity difference $U_{Bc}(z,t)$ between the surface and a deeper level, z, horizontally averaged between the two stations by using the traditional dynamical method. Here we choose the deeper level to be at 600 m depth. If the two standard stations are between altimetry points A_k and A_{k+1} then the Altimetric offset for that interval may be estimated from an expression similar to Eq. (7):

$$U_k^0 = \langle U_{Bc}(600,t) - \frac{g}{f \cdot L} \cdot \Delta H_k(t) \rangle + \langle U_k(600,t') \rangle \equiv \langle X \rangle_g + \langle Y \rangle_{600} \qquad (18)$$

where $\langle\ \rangle$ again indicates temporal averaging and we have used two different averages and two different time labels (t and t') to indicate that the baroclinic velocity difference $U_{Bc}(600,t)$ and the velocity at 600 m depth $U_k(600,t')$ usually have not been measured at the same time.

The use of baroclinic velocity for estimating U_k^0 is mainly relevant north of altimetry point A_5, where we only have few ADCP deployments and the fifth column in Table 7 lists values for the first average on the right-hand side of Eq. (18) using the pairs of CTD standard stations that would seem to represent the altimetry intervals best. The last column in the table is calculated from the ADCP velocities at 600 m depth at sites NC and NH.

Table 7. The last two columns in the table show values for the two averages in Eq. (18) and their 95% confidence intervals for the three northernmost altimetry intervals. "N" is the number of baroclinic profiles in each CTD station interval in the altimetry period (since 1993). "R" is the correlation coefficient between $U_{Bc}(600,t)$ and $\Delta H_k(t)$ with statistical significance level. The values in the last column are based on ADCP measurements at site NC for interval A_5-A_6 and at site NH for interval A_6-A_7.

Alt.interval	CTD st.	N	R	$\langle X \rangle_g$ cm/s	$\langle Y \rangle_{600}$ cm/s
A_5–A_6	N06–N07	99	0.50***	9.1±2.3	0.2±1.8
A_6–A_7	N07–N09	99	0.66***	9.4±1.4	0.3±2.7
A_7–A_8	N09–N10	96	0.44***	2.0±1.5	

3.6 The Altimetric offsets

We now have the necessary input to estimate updated values for the Altimetric offsets U_k^0 for $k = 2$–7 to replace the values in H2015 Table S2.4.4. To give the best fit with surface velocity from ADCPs between A_3 and A_5, we use the values in Eq. (11b) and Eq. (14). In the interval between A_2 and A_3, we only consider the northern half, north of standard station N02 at 62.5°N. ADCP site NI was located in this interval and is considered the best evidence. To get a value for U_2^0 that may be considered an average between N02 and A_3, the line between NA and NI is extrapolated southwards to N02 (dashed line in Figure 10) and the average calculated from that.
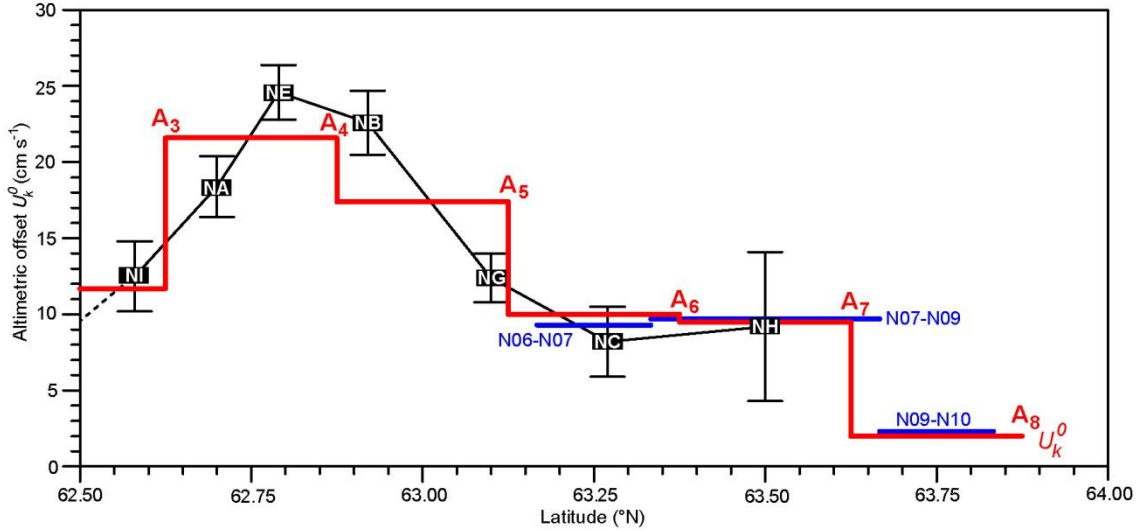
Figure 10. The chosen values for the Altimetric offset for surface velocity in each altimetry interval are shown by the red lines. Black rectangles with ADCP site names indicate U_k^0 values derived from individual ADCP sites with error bars indicating 95% confidence intervals (Table 6). Blue lines indicate U_k^0 values derived from CTD data and measurements of deep currents using Eq. (18) (Table 7).

Between A_5 and A_7, U_k^0 values may be estimated from the measurements at ADCP sites NG, NC, and NH (Table 6) as well as from the CTD measurements between N06 and N09 (Table 7). As illustrated in Figure 10, these two different methods are fairly consistent. Our choice, as shown by the red line in Figure 10, is a compromise between the two methods. For the last altimetry interval, between A_7 and A_8, there are no ADCP measurements and the value for U_7^0 is determined from the CTD measurements (Table 7) where we assume that the value for $\langle Y \rangle_{600}$ has a similar magnitude as for the other two rows in the table. The chosen values for U_k^0 are listed in Table 8 in the row, labelled "Surface" U_k^0.

Table 8. Values for the Altimetric offset U_k^0 (in cm s^{-1}) between points A_2 and A_8. "H2015" U_k^0 values are those used in H2015 (Table S2.4.4). "Surface" U_k^0 values are the new values that give the best fit for the surface velocity, derived as described above (red lines in Figure 10). "Transport" U_k^0 values are adjusted for horizontal velocity variations within altimetry intervals (Sect. 3.7) to give values that may be more suitable for calculating volume transport rather than surface velocity. The last column lists the average volume transport 1993-2017 with each set of Altimetric offsets while other parameters were kept to their values in H2015.

Interval:	A_2–A_3	A_3–A_4	A_4–A_5	A_5–A_6	A_6–A_7	A_7–A_8	Vol. Tr.
"H2015" U_k^0:	11	21	18	11	10	3	3.83 Sv
"Surface" U_k^0:	11.7	21.6	17.4	10	9.5	2	3.73 Sv
"Transport" U_k^0:	12.5	21.9	17.7	10	9.5	2	3.78 Sv

3.7 Horizontal velocity variation within altimetry intervals

The Altimetric offset value U_k^0 for the interval between points A_k and A_{k+1}, as derived above, is designed to give as good a value as possible for the surface velocity, $U_k(0,t)$, when used in Eq. (1). As illustrated in Figure 10, the surface velocity may vary laterally within the interval, but the chosen value is designed to be an optimal choice for the horizontally averaged surface velocity between the two points. This may not, however, always be the best choice when computing transport values.

As an example, consider the interval between points A_3 and A_4. The Altimetric offset for this interval, U_3^0, was determined from ADCP sites NA, NE, and NB by Eq. (13) with the weighting factors $\gamma_{NA} = 0.31$, $\gamma_{NE} = 0.32$, and $\gamma_{NB} = 0.37$. Thus, all three ADCP sites count almost equally, but when the velocity is integrated vertically, site NA ought to contribute less, because it is shallower than the other sites. Also, the velocity profile may be different at different sites. To take this into account, we define a new parameter, "Equivalent depth", D_{Eq}, which may be associated with each ADCP site:

$$D_{Eq} \cdot \langle U(0,t) \rangle \equiv \langle \int_0^{D_{Atl}} U(z,t) dz \rangle \qquad (19)$$

where $\langle\ \rangle$ again indicates temporal averaging, $U(z,t)$ is the velocity measured by the ADCP at depth z and time t, and D_{Atl} is the average depth of the Atlantic layer at the site. For sites NI and NA, D_{Atl} is the bottom depth. For the other sites, D_{Atl} is the average depth of the Atlantic layer, as defined by the average 4°C-isotherm, at the site (Figure 1b). In plain words, D_{Eq} is the value by which to multiply the average surface velocity to give the average vertical integral over the Atlantic layer and it is easily calculated for each site from the ADCP measurements (Table 9).

Table 9. Equivalent depth of the various ADCP sites as defined by Eq. (19).

Site:	NI	NA	NE	NB	NG	NC	NH
D_{Eq}:	140m	261m	349m	283m	245m	203m	142m

If we use the values in Table 9 to determine how much each of the three ADCP sites should count in Eq. (13), the weighing factors become $\gamma_{NA} = 0.29$, $\gamma_{NE} = 0.39$, and $\gamma_{NB} = 0.32$. The value for U_3^0 would then change from 21.6 cm s^{-1} to 21.9 cm s^{-1} (Table 8). Similarly, the value for U_4^0 would change from 17.4 cm s^{-1} to 17.7 cm s^{-1} (Table 8). For both these altimetry intervals, the changes are small – well within the uncertainties. For U_2^0, we choose the value for NI in Table 6 since it is slightly displaced from the middle of the altimetry interval towards the deep end

To see the effect of choosing different U_k^0 values on transport, the average volume transport for the period from 1 Jan 1993 to 31 Dec 2017 has been calculated with the different values in Table 8, but no other changes relative to the H2015 algorithm. The result (last column in Table 8) shows that the effect on the average volume transport is much less than the quoted uncertainty (0.5 Sv). The three time series of monthly averaged transport for this period were also highly correlated with all of the correlation coefficients being equal to or exceeding 0.998***.

4 The vertical variation of eastward velocity

4.1 Vertical integration

Once the eastward velocity has been determined in the surface for the various altimetry intervals on the section, it remains to determine its vertical variation down through the Atlantic layer. Here, we again use the ADCP data and utilize the fact that the velocity variations are fairly barotropic, especially in the upper parts of the Atlantic layer. As a first approximation, we therefore test the assumption that the eastward velocity $U(z,t)$ at depth z and time t at a certain ADCP site is proportional to the simultaneous surface velocity, $U(0,t)$, at the site:

$$U(z,t) \cong U(0,t) \cdot \varphi_0(z) \qquad (20)$$

where the proportionality factor, $\varphi_0(z)$, varies with depth, but not with time, and may be determined for any depth by a regression analysis requiring zero offset:

$$\varphi_0(z) = \frac{\sum_t U(0,t) \cdot U(z,t)}{\sum_t U(0,t) \cdot U(0,t)} \qquad (21)$$

We will mainly consider variations at monthly time scales and will use ADCP velocities averaged over 28 consecutive days. The fraction of the variance of $U(z,t)$ that is explained by Eq. (20) will generally decrease with depth, but remains fairly high in the upper layers. Since the eastward velocity is to be integrated vertically to get transport time series, a better estimator of the fit in Eq. (20) may be to consider the integral of $U(z,t)$ from the surface down to some depth, D. If Eq. (20) is approximately valid, then this integral should also be approximately proportional to the surface velocity:

$$\Gamma(D,t) \equiv \int_0^D U(z,t)dz \cong U(0,t) \cdot \int_0^D \varphi_0(z)\,dz \qquad (22)$$

As an indicator of the validity of this approximation, we may then use the correlation coefficient, R_D, between $\Gamma(D,t)$ and $U(0,t)$. In Table 10, this correlation coefficient is listed for two different depths for the deep ADCP sites. We are mainly interested in the transport of Atlantic water, which on average extends from the surface down to a depth, D_A, listed in the first row of Table 10. The correlation coefficients, R_A, between surface velocity and the integral down to this depth are listed in the fourth row of the table. For the three southernmost sites, the average Atlantic layer extends all the way (at sites NI and NA) or very close (site NE) to the bottom and deeper than the maximum depth with complete ADCP data coverage, D_M. For these sites, the velocities at depth D_M are extended to the bottom depth.

Except for site NA, R_A is seen to be above 0.96 and quite close to 1 for the four northernmost sites. The Atlantic layer thickness at a given location does, however, vary and may extend considerably deeper than D_A. Table 10 therefore also lists the correlation coefficients, R_D, at 600 m depth.

Table 10. Average Atlantic water depth (D_A) at the ADCP sites, maximum depth (D_M) of complete data coverage, number of 28-day averaged values (N) at each site, and correlation coefficient between surface velocity and integrated velocity down to depth D_A (R_A, fourth row), and down to 600 m depth for the deep sites (R_D, fifth row). For sites NI, NA, and NE, the velocities measured at depth D_M have been extended down to the bottom. For sites NG and NC, velocities have likewise been extended from depth D_M down to 600 m.

Site:	NI	NA	NE	NB	NG	NC	NH
D_A (m):	156	300	428	362	301	255	151
D_M (m)	139	275	418	623	588	586	615
N:	12	231	95	253	167	53	12
R_A:	0.969*	0.898***	0.973***	0.986***	0.988***	0.989***	0.998***
R_D:				0.950***	0.974***	0.960***	0.970***

4.2 Seasonal variation

The high correlations in Table 10 indicate that Eq. (20) for most of the sites provides a good approximation. For some of the sites, the fit is not so good, however, and especially site NA has a lower correlation coefficient. The main reason for this appears to be that the profile of the eastward velocity at this site has a strong seasonal variation. As seen in Figure 3, the velocity structure at NA is almost barotropic in winter, but has a strong baroclinic component in late summer.

To account for this, the correlation coefficients between $\Gamma(D_A,t)$ and $U(0,t)$ have been calculated separately for individual months (Figure 11a) for the four ADCP sites with the longest records. To get adequate statistics, the values for each month are based on a 3-month period centred on that month. As seen in Figure 11a, the correlation coefficients for NA vary through the season, but the lowest value (0.922 in December) is still higher than the annual value in Table 10 (0.898). This seasonality is also seen for $\Gamma(D_A,t)$ in Figure 11b, which shows that for NA, $\Gamma(D_A,t)$ is 43% higher in March than in October.

For the three other long-term sites, the seasonal variation of the correlation coefficient in Figure 11a is smaller, except that site NE has an abnormal value in May. This does not, however, seem to have affected the value for $\Gamma(D_A,t)$ in May (Figure 11b) and generally these three sites have smaller variations in $\Gamma(D_A,t)$ than site NA.
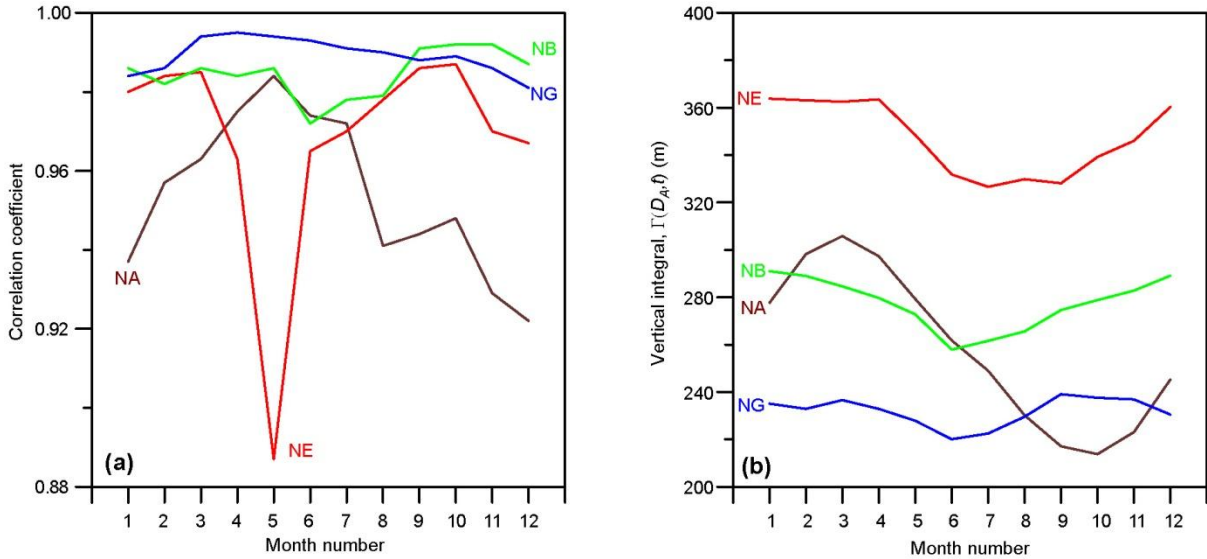
Figure 11. Seasonal variation of the correlation coefficient between the eastward surface velocity and the vertical integral down to the average depth of the Atlantic layer, $\Gamma(D_A,t)$, **(a)** and seasonal variation of $\Gamma(D_A,t)$ **(b)** for the four long-term ADCP sites. The plots are based on 28-day averaged velocities and the values for each month are based on that month as well as the preceding and the following months.

The high correlations in Table 10 and Figure 11a verify that Eq. (20) is a good approximation and it would seem appropriate to generate the integrals on the right hand side of Eq. (22) for the altimetry intervals to use in calculations of transport. The deep boundary of the Atlantic water layer on the section is generally not horizontal, however, and will vary within altimetry intervals. We therefore return to Eq. (20) and have calculated values for the proportionality factor $\varphi_0(z)$ for every meter from the surface down to the bottom or 600 m for all the selected ADCP sites using Eq. (21).

To account for the seasonality evident for some of the sites in Figure 11b, the calculation has also been done for individual months, based on 3-month averages, to generate proportionality factors $\varphi_m(z)$ for each month m = 1,...,12, although that is only meaningful for the four long-term sites where several years of data are available. These proportionality factors for individual ADCP sites have then been combined to generate proportionality factors, $\Phi_{k,m}(z)$, for each altimetry interval $A_k - A_{k+1}$ and

each month m (Figure 12). From Table 10 and Figure 11, the seasonal variation is most pronounced for the southernmost half of the section. For the northernmost half, there are only two ADCP sites, NC and NH, neither of which has many years of observations and the annual averages for these sites provide good approximations according to Table 10. For the three northernmost altimetry intervals, the proportionality factors, $\Phi_{k,m}(z)$, are therefore assumed not to vary with season.
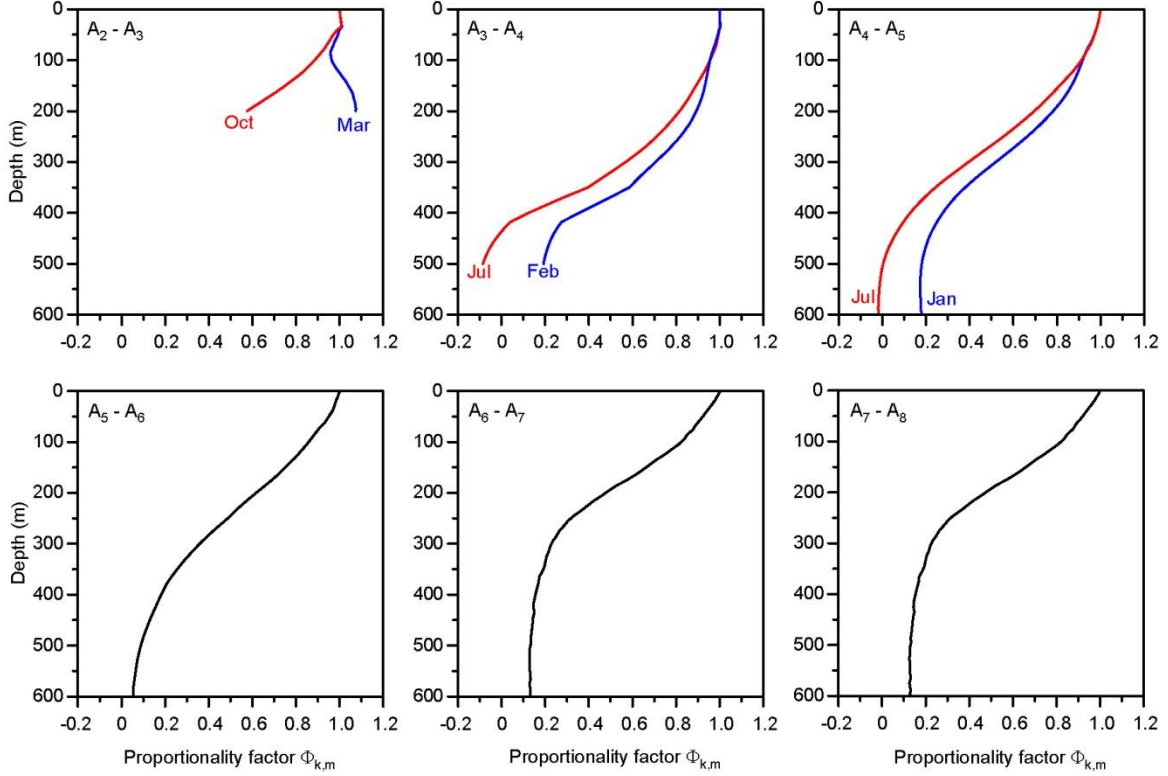
Figure 12. Proportionality factors for the six altimetry intervals. For the three northernmost intervals (bottom row of panels), the annually averaged proportionality factors for individual ADCP sites were used. Thus, $\varphi_0(z)$ for site NC was used to generate the factor, $\Phi_{5,0}(z)$, for the altimetry interval $A_5 - A_6$, whereas $\varphi_0(z)$ for site NH was used to generate the factors, $\Phi_{6,0}(z)$ and $\Phi_{7,0}(z)$, for intervals $A_6 - A_7$, and $A_7 - A_8$, respectively. For the three southernmost intervals (top row of panels), individual factors, $\Phi_{k,m}(z)$, were generated for each month and each panel only shows the factors for the two most extreme months. For the interval $A_2 - A_3$, we have used the $\varphi_m(z)$ factors from site NA. For the interval $A_3 - A_4$, the $\varphi_m(z)$ factors from site NA, NE, and NB have been combined as in Eq. (13) with the same values ($\gamma_{NA} = 0.31$, $\gamma_{NE} = 0.32$, and $\gamma_{NB} = 0.37$) in the surface, but changing with depth, first by reducing γ_{NA} and increasing γ_{NE} accordingly down to the maximum depth (275 m) of NA, then reducing γ_{NE} and increasing γ_{NB} down to the maximum depth (418 m) of NE, after which only NB remains. For the interval $A_4 - A_5$, the $\varphi_m(z)$ factors from site NB and NG have been combined as in Eq. (8) with the same values ($\beta_{NB} = 0.51$ and $\beta_{NG} = 0.49$) from the surface down to 600 m depth.

With the proportionality factors, $\Phi_{k,m}(z)$, for each altimetry interval, k, and month, m, determined, Eq. (1) may be extended to explain the full velocity structure on the monitoring section in terms of altimetry:

$$U_k(z,t) = \Phi_{k,m}(z) \cdot U_k(0,t) = \Phi_{k,m}(z) \cdot \left[\frac{g}{f \cdot L} \cdot \Delta H_k(t) + U_k^0 \right] \qquad (23)$$

where $U_k(z,t)$ is the velocity at depth z and time t (within month m) horizontally averaged within altimetry interval $A_k - A_{k+1}$. To a good approximation, the whole velocity field may thus be derived from the differences in sea level anomaly (SLA), $\Delta H_k(t)$, between neighbouring altimetry points.

4.3 Volume transport calculation

We now have all the necessary information to estimate volume transport. Most generally, we will want to calculate the volume transport, $Q(t)$, between altimetry points A_2 and A_8 from the surface down to some level, $D_k(t)$, where the index k refers to the altimetry interval and the deep boundary may vary with time. The volume transport of Atlantic water may be estimated as:

$$Q(t) = \sum_{k=2}^{7} W_k \cdot \left\{ \int_{z=0}^{600m} [w_k(z,t) \cdot U_k(z,t)] \; dz \right\} \qquad (24)$$

where $U_k(z,t)$ as before is the eastward velocity at depth z and time t, horizontally averaged over altimetry interval k (between A_k and A_{k+1}). W_k is the distance between the two altimetry points and is 27.87 km, except for the southernmost interval where W_2 is only half of this, since the southern half of this interval is considered part of the semi-closed shelf circulation. $w_k(z,t)$ is the fraction of water at depth z in altimetry interval k that is above the lower boundary of the Atlantic layer at time t. To calculate the average volume transport of Atlantic water for a specific year, y, and month m, Eq. (23) is used to express $U_k(z,t)$ within Eq. (24):

$$Q_{y,m} = \sum_{k=2}^{7} W_k \cdot \left[\frac{g}{f \cdot L} \cdot \Delta H_{k,y,m} + U_k^0 \right] \cdot \left\{ \int_{z=0}^{600m} [w_{k,y,m}(z) \cdot \Phi_{k,m}(z)] \; dz \right\} \qquad (25)$$

where $\Delta H_{k,y,m}$ is the SLA difference across altimetry interval $A_k - A_{k+1}$, $\Delta H_k(t)$, averaged over the month m in year y. When altimetry data are available for a period, Eq. (25) allows calculation of $Q_{y,m}$ for every year and month within the period as long as estimates for the monthly averaged width, $w_{k,y,m}(z)$ are available. Since the lower boundary of the Atlantic layer in H2015 is defined by temperature and salinity (4°C isotherm and 35.0 isohaline), this requires knowledge of the hydrography, which has not been addressed in this report.

If we use the algorithms for the hydrographic fields developed in H2015 to calculate $w_{k,y,m}(z)$, new transport estimates may be calculated from Eq. (25). In Figure 13, this method has been used to re-calculate the volume transport for the period covered in H2015 and the "New" transport series compared with the "Old" series. The correlation is seen to be high and the "New" average transport for this period was 3.84 Sv compared to the "Old" average: 3.82 Sv, i.e. a difference around 0.5%.
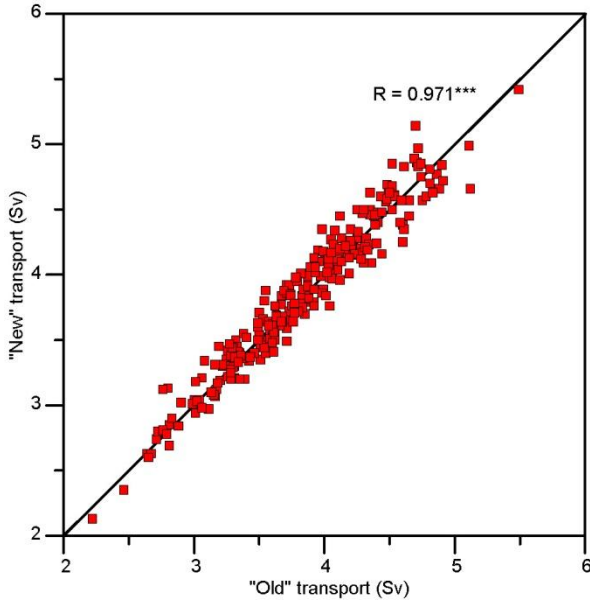
Figure 13. Monthly averaged volume transport of Atlantic water, computed by the new algorithms ("New" transport), where we have used the row labelled "Transport" U_k^0 in Table 8, plotted against the transport time series reported in H2015 ("Old" transport) for the period January 1993 to April 2014. The correlation coefficient is indicated and the diagonal line indicates equality.

5 Discussion

The Faroe Current is the strongest branch of Atlantic inflow to the Arctic Mediterranean (Østerhus et al., 2019) and the Faroe Marine Research Institute considers it an important task to monitor its volume transport as well as transports of heat and salt and continue the time series that now span more than two decades.

In the early phase, the monitoring relied heavily on the array of moored ADCPs (Figure 1b, Table 1, Table A1), which to a large extent were acquired and maintained by external funding, but continued reliance on this type of funding proved difficult and the early results indicated good correspondence between transport derived from in situ measurements and sea level tilt derived from satellite altimetry (Hansen et al., 2010). In an attempt to make the monitoring system more sustainable, investigations were therefore initiated to determine how much the resource-demanding in situ monitoring could be replaced by satellite altimetry.

The initial results of these investigations were reported in Hansen et al. (2015), H2015, where it was suggested that altimetry data could replace much of the observations acquired by moored ADCPs, once the altimetry data had been calibrated against in situ observations. There were still open questions, however, which led to the additional in situ observations, funded by FARMON, and the analyses reported here. In this report, we aim to document the results of these analyses and answer some of the questions as detailed below.

- *How well do sea level anomalies (SLA-values) from satellite altimetry represent variations in surface velocity?* This question is addressed in Sect. 3.4 where it is found that over the central (and most important) part of the monitoring section, variations in SLA differences between altimetry points can explain at least 74% of the variance in horizontally averaged surface velocity perpendicular to the section. It was furthermore suggested that much of the remaining discrepancy between altimetry and in situ measurements might as well be due to uncertainty in the in situ observations rather than the altimetry data. This conclusion is partly from the low positive correlations between neighbouring ADCP sites and partly from the significant negative correlations between ADCP sites in the central part of the section and its ends. Comparing the result for Eq. (16) with the values in Table 4 and Table 5, it appears that an ADCP array would need to have considerably better horizontal resolution than our old in situ system (Figure 1b) if it were to give better horizontally averaged surface velocities than altimetry. Thus, a monitoring system for the Faroe Current, based only on in situ observations, would probably need on the order of ten ADCP moorings, at least two of which would have to be within expensive frames to protect them from fisheries.

- *How well can altimetry data be calibrated to give, not only variations, but also the absolute values for surface velocity?* Calibration of SLA-values to give absolute surface velocity involves determination of the Altimetric offsets, U_k^0, in Eq. (1) and is necessary because available values for Mean Dynamic Topography seem to be too smooth to be realistic (H2015). Using individual ADCP sites, the uncertainties (95% confidence intervals) in the U_k^0 values were in most cases around 2 cm s^{-1} (Table 6). For the interval between A$_3$ and A$_5$, through which most of the Atlantic water passes, combinations of ADCP sites gave U_k^0 values with uncertainties around 1 cm s^{-1}, Eq. (10) and Eq. (14), which is around 5% of the U_k^0 values. For the other altimetry intervals, the relative uncertainty is considerably higher (Table 6 and Table 7). The derivations of U_k^0 values are also critically dependent on the assumptions and approximations made in extrapolating ADCP velocities to the surface, such as the barotropic character of velocity variations, Eq. (2), and geostrophy in the near-surface

layer, Eq. (6). Uncertainties in the U_k^0 values translate directly into volume transport and we conclude that the uncertainty in average Atlantic water volume transport from this source is at least 5% i.e. 0.2 Sv. This is almost half the quoted total uncertainty of 0.5 Sv (H2015), but it should be emphasized that an error in the U_k^0 values is in the form of a bias, which will affect average values for transport, but will have little or no effect on transport variations or trend estimates.

- ***How well can vertical profiles and transport be determined from surface velocity and altimetry data?*** This question may be translated into asking how good an approximation Eq. (20) is. From Table 10 and Figure 11, the answer seems to be that this approximation explains around 90% of the variance in Atlantic water volume transport (squared correlation coefficients). Again, it may be argued that part of this explanatory power comes from the assumption of barotropic velocity variations, Eq. (2), used to extrapolate ADCP velocities to the surface. This is certainly the case, but the same problem would also arise for a monitoring system, based on moored ADCPs, which also would need to be extrapolated to the surface.

Summarizing this discussion, we conclude that a monitoring system based solely on satellite altimetry can explain the variations in the velocity structure of the Faroe Current as well as a system based on an array of ADCP moorings, and probably more accurately unless the ADCP array were to have a considerably better horizontal resolution (i.e. more ADCPs) than our original system.

This conclusion can only be reached, however, because we have had access to the extensive set of ADCP and CTD measurements acquired since the monitoring began in the 1990s. Without these data, determination of the U_k^0 values (Table 8) and the proportionality factors $\Phi_{k,m}(z)$ (Figure 12) would not have been possible. From the relative uncertainties (confidence interval divided by average value) of the U_k^0 values of the various ADCP sites in Table 6, we also see the value of having many deployments and long time series at a site. At the same time, these relative uncertainties indicate, however, that considerable efforts would be required if we wanted to reduce the overall transport uncertainty by added future in situ observations.

From the results in this study, the algorithms developed in H2015 have been modified by new values for U_k^0 and $\Phi_{k,m}(z)$ and better account of seasonal variations has been achieved. Future releases of time series will therefore be different from previous releases, also for historic values all the way back to 1993, but the differences are slight. For the U_k^0 values, this is seen in Table 8 and for Atlantic water transport; this is verified in Sect. 4.3. For the period addressed in H2015 (Jan 1993 to April 2014), the new algorithm increased the average transport from 3.82 Sv to 3.84 Sv, i.e. by an order of magnitude less than the quoted uncertainty (0.5 Sv). The correlation between monthly averaged "New" and "Old" transport values was also high (0,971***) and no individual month had a deviation of more than 0.5 Sv between "Old" and "New" transport (Figure 13).

For the future monitoring system, the results of this study confirm the suggestion in H2015 that ADCP measurements are not necessary to monitor the velocity structure on the section. There are two caveats, however. The first caveat is that monitoring Atlantic water transport on this section also requires monitoring of the temperature and salinity fields, which does require in situ observations, at least presently. This question will be addressed in a report, planned to be finalized later in 2019.

The second caveat is that the new algorithms have been developed from measurements over the last two decades, during which the Faroe Current has remained remarkably stable (H2015). As long as it continues to do so and the quality of satellite altimetry in this region persists, the algorithms ought to remain valid, but potential major changes to the system might invalidate them.

If global warming were to induce a future weakening of the Atlantic inflow, as some climate models project under some scenarios, we would expect a signal in the satellite altimetry, but there might also be changes in the subsurface velocity field, not obvious in the altimetry data or the altimetry data might degrade in quality for some reason. To guard against this possibility, we recommend that an ADCP mooring is maintained at one of the long-term ADCP sites and the obvious choice would be site NB, both because of its length (Table 1) and because of its ability to represent surface velocity over larger scales (e.g. Eq.(16)).

Taking into account the negative correlation coefficients in Table 4 and Table 5, one should not expect data from any single ADCP site to represent volume transport with high accuracy and that is not the case for site NB either, but there is some correspondence as shown in Figure 14. To produce this figure, all the months with complete coverage at site NB were selected and average velocity calculated for the depth interval covered by all the deployments. For monthly averages (open squares in Figure 14), the correlation coefficient was 0.52***. For averages over ten months (red circles in Figure 14), the correlation coefficient increased to 0.61*.

Thus the eastward velocity at this site is an indicator of volume transport, although not very sensitive. We therefore recommend that the long-term ADCP site NB, which has been occupied almost continuously since 1997 (Table A1), is retained in the future monitoring system.
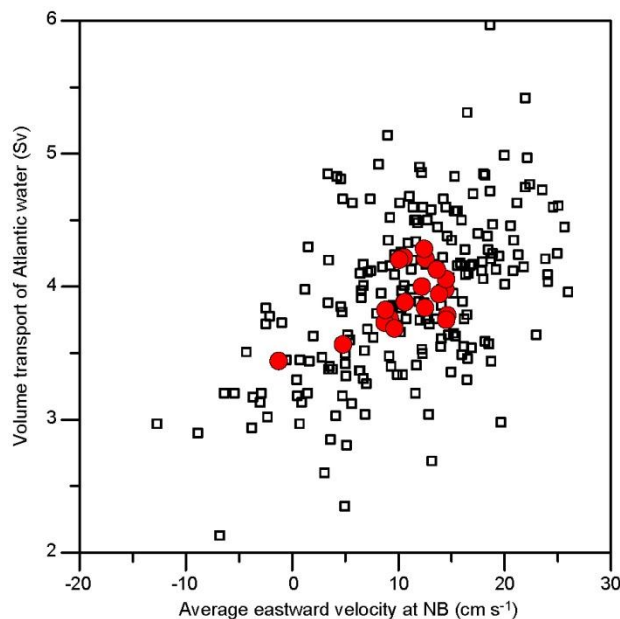
Figure 14. Volume transport of Atlantic water plotted against the eastward velocity at site NB averaged between 262 and 362 m depth. Open squares represent monthly averages. Red circles represent averages over ten months (not necessarily contiguous).

References

Hansen, B., Hátún, H., Kristiansen, R., Olsen, S. M., and Østerhus, S.: Stability and forcing of the Iceland-Faroe inflow of water, heat, and salt to the Arctic, Ocean Science, 6, 1013-1026, 10.5194/os-6-1013-2010, 2010.

Hansen, B., Larsen, K. M. H., Hátún, H., Kristiansen, R., Mortensen, E., and Østerhus, S.: Transport of volume, heat, and salt towards the Arctic in the Faroe Current 1993–2013, Ocean Science, 11, 743-757, 10.5194/os-11-743-2015, 2015.

Pyper, B. J. and Peterman, R. M.: Comparison of methods to account for autocorrelation in correlation analyses of fish data, Can. J. Fish. Aquat. Sci., 55, 2127–2140, https://doi.org/10.1139/f98-104, 1998.

von Storch H.: Misuses of Statistical Analysis in Climate Research. In: von Storch, H., Navarra, A. (eds) Analysis of Climate Variability. Springer, Berlin, Heidelberg, 1999.

Østerhus, S., R. Woodgate, H. Valdimarsson, B. Turrell, L. de Steur, D. Quadfasel, S. M. Olsen, M. Moritz, C.M. Lee, K.M.H. Larsen, S. Jónsson, C. Johnson, K. Jochumsen, B. Hansen, B. Curry, S. Cunningham, and B. Berx.: Arctic Mediterranean exchanges: a consistent volume budget and trends in transports from two decades of observations. Ocean Sci., 15, 379–399, 2019.

Table A1. Details of ADCP deployments on the N-section. "Lgt" is bin length (m). "Last" is the highest (shallowest) level reached by the ADCP. "Top" is the highest level with 100% good daily-averaged data.

Deploym.	Position Lat.	Long.	Botm (m)	Period yyyymmdd-yyyymmdd	Dur. Days	Bins Lgt	Last	Top	Depths(m) Bin1	Last	Top
NWNI1706	62.5827	-6.0877	156	20170610-20180517	342	10	11	7	139	39	79
NWNA9601	62.7062	-6.0885	302	19960125-19960525	122	10	21	20	287	87	97
NWNA9606	62.6988	-6.0778	292	19960617-19970521	339	10	25	17	275	35	115
NWNA9706	62.7052	-6.0862	300	19970615-19980608	359	10	24	19	283	53	103
NWNA9807	62.7030	-6.0841	297	19980708-19990701	359	10	24	18	280	50	110
NWNA9907	62.6991	-6.0648	295	19990703-20000615	349	10	24	17	278	48	118
NWNA0007	62.7008	-6.0743	297	20000708-20010615	343	10	24	18	280	50	110
NWNA0107	62.7017	-6.0683	298	20010707-20020613	342	10	23	15	281	61	141
NWNA0207	62.7033	-6.0722	301	20020706-20030613	343	10	24	15	284	54	144
NWNA0307	62.6999	-6.0811	294	20030705-20040610	342	10	23	16	277	57	127
NWNA0407	62.7003	-6.0845	293	20040703-20050519	321	10	25	19	276	36	96
NWNA0506	62.6991	-6.0719	303	20050612-20060522	345	10	24	18	286	56	116
NWNA0606	62.7051	-6.0783	304	20060610-20070517	342	10	25	20	287	47	97
NWNA0706	62.7034	-6.0785	303	20070609-20080517	344	10	24	18	286	56	116
NWNA0806	62.6999	-6.0852	296	20080606-20090514	343	10	24	17	279	49	119
NWNA0906	62.6997	-6.0852	301	20090606-20100513	342	10	24	18	284	54	114
NWNA1006	62.7013	-6.0800	298	20100605-20110519	349	10	23	16	281	61	131
NWNA1106	62.7028	-6.0846	298	20110611-20120519	344	10	23	14	281	61	151
NWNA1206	62.7033	-6.0817	300	20120608-20130516	343	10	24	16	283	53	133
NWNA1306	62.7006	-6.0768	300	20130610-20140514	339	10	24	17	283	53	123
NWNA1406	62.7025	-6.0842	300	20140606-20150524	353	10	24	16	283	53	133
NWNE0007	62.7915	-6.0850	456	20000707-20010615	344	25	15	11	424	74	174
NWNE0407	62.7918	-6.0892	455	20040703-20050519	321	25	15	13	432	82	132
NWNE0506	62.7907	-6.0737	456	20050612-20060522	345	25	15	13	424	74	124
NWNE0606	62.7964	-6.0763	462	20060610-20070517	342	25	15	13	431	81	131
NWNE0706	62.7904	-6.0843	450	20070609-20080517	344	25	14	13	418	93	118
NWNE0806	62.7939	-6.0817	457	20080607-20090514	342	25	15	13	425	75	125
NWNE0906	62.7938	-6.0819	455	20090606-20100513	342	25	15	13	423	73	123
NWNE1006	62.7932	-6.0830	456	20100605-20110519	349	25	14	12	424	99	149
NWNF0007	62.8783	-6.0838	697	20000708-20010615	343	25	24	19	653	78	203
NWNB9410	62.9181	-6.0772	962	19941023-19950216	117	25	23	21	624	74	124
NWNB9706	62.9136	-6.0826	907	19970614-19980612	364	25	23	18	623	73	198
NWNB9807	62.9193	-6.0807	961	19980705-19990618	349	25	25	20	672	72	197
NWNB9907	62.9169	-6.0875	947	19990703-19990706	4	25	24	24	669	94	94
NWNB9908	62.9189	-6.0842	957	19990821-20000615	300	25	25	19	679	79	229
NWNB0007	62.9184	-6.0837	954	20000708-20010615	343	25	24	19	676	101	226
NWNB0107	62.9210	-6.0852	980	20010707-20020614	343	25	25	19	702	102	252
NWNB0207	62.9211	-6.0853	981	20020706-20030613	343	25	25	21	703	103	203
NWNB0307	62.9171	-6.0852	955	20030706-20040610	341	25	24	20	665	90	190
NWNB0407	62.9214	-6.0817	987	20040703-20050519	321	25	25	20	697	97	222
NWNB0506	62.9174	-6.0841	956	20050612-20060126	229	25	23	19	666	116	216
NWNB0602	62.9157	-6.0900	942	20060217-20060521	94	25	19	18	652	202	227
NWNB0606	62.9080	-6.0827	958	20060610-20070517	342	25	22	19	669	144	219
NWNB0706	62.9166	-6.0828	955	20070609-20080517	344	25	23	20	666	116	191
NWNB0806	62.9183	-6.0867	953	20080607-20090514	342	25	23	19	664	114	214
NWNB0906	62.9183	-6.0850	959	20090606-20100513	342	25	23	20	670	120	195
NWNB1006	62.9177	-6.0858	961	20100605-20110519	349	25	23	18	672	122	247
NWNB1106	62.9158	-6.0834	951	20110611-20120519	344	25	23	17	662	112	262
NWNB1206	62.9200	-6.0800	961	20120609-20130516	342	25	23	19	671	121	221
NWNB1306	62.9117	-6.0822	964	20130610-20140514	339	10	62	55	691	81	151
NWNB1406	62.9160	-6.0835	958	20140607-20150524	352	10	62	54	686	76	156
NWNB1506	62.9167	-6.0833	947	20150615-20160518	339	25	22	19	657	132	207
NWNB1606	62.9178	-6.0829	968	20160609-20170521	347	25	24	21	678	103	178
NWNB1706	62.9185	-6.0817	961	20170610-20180517	342	25	23	19	674	124	224

Table A1 continued.

Deploym.	Position		Botm	Period	Dur.	Bins			Depths(m)		
	Lat.	Long.	(m)	yyyymmdd-yyyymmdd	Days	Lgt	Last	Top	Bin1	Last	Top
NWND9711	62.9590	-6.0933	1283	19971112-19980612	213	25	23	17	634	84	234
NWNG0007	63.0993	-6.0836	1816	20000708-20010615	343	25	22	19	607	82	157
NWNG0107	63.1057	-6.0817	1811	20010707-20020613	342	25	22	17	602	77	202
NWNG0207	63.1049	-6.0819	1801	20020706-20030613	343	25	22	17	592	67	192
NWNG0307	63.1016	-6.0838	1799	20030706-20040610	341	25	21	20	590	90	115
NWNG0407	63.0973	-6.0867	1798	20040703-20050519	321	25	22	20	588	63	113
NWNG0506	63.1063	-6.0845	1803	20050612-20060521	344	25	22	20	593	68	118
NWNG0606	63.1030	-6.0850	1808	20060610-20070517	342	25	22	20	605	80	130
NWNG0706	63.0995	-6.0837	1804	20070609-20080517	344	25	22	20	601	76	126
NWNG0806	63.1013	-6.0843	1796	20080607-20090514	342	25	22	21	593	68	93
NWNG0906	63.1050	-6.0833	1810	20090606-20100513	342	25	22	21	607	82	107
NWNG1006	63.1000	-6.0833	1796	20100605-20110519	349	25	22	17	593	68	193
NWNG1106	63.1000	-6.0833	1813	20110611-20120519	344	25	22	18	610	85	185
NWNG1306	63.0967	-6.1017	1808	20130610-20140514	339	25	21	16	604	104	229
NWNG1406	63.1000	-6.0833	1802	20140607-20150524	352	25	22	17	598	73	198
NWNC9410	63.2725	-6.1050	1730	19941023-19950216	117	25	22	19	586	61	136
NWNC9606	63.2680	-6.1085	1731	19960617-19970521	339	25	22	19	604	79	154
NWNC9706	63.2738	-6.1100	1733	19970614-19980612	364	25	23	18	623	73	198
NWNC9807	63.2657	-6.1050	1728	19980706-19990618	348	25	22	18	619	94	194
NWNC9907	63.2653	-6.1065	1740	19990703-20000615	349	25	23	19	631	81	181
NWNH1506	63.5037	-6.0765	1802	20150615-20160518	339	10	56	49	615	65	135